

Cyclone Hudhud-eddy induced phytoplankton bloom in the northern Bay of Bengal using a coupled model

P. J. Vidya^{1,3*}, M. Balaji² and Mani Murali R¹

¹CSIR-National Institute of Oceanography,
Dona Paula, Goa-403 004, India.

²Centre for Oceans, Rivers, Atmosphere, and Land Sciences,
Indian Institute of Technology Kharagpur-721302, West Bengal, India.

³Present address: National Centre for Polar and Ocean Research,
Ministry of Earth Sciences (MoES), Headland Sada, Goa-403 804, India.

*Corresponding author: vidya@ncpor.res.in; pjvidya@gmail.com

Abstract

The present study explored the role of the pre-existing cyclonic eddy on the chlorophyll-a (Chl_a) bloom after a cyclone pass over the northern Bay of Bengal (BoB). We used a high-resolution (~9 km) Regional Ocean Modeling System (ROMS) coupled with an established Nutrient-Phytoplankton-Zooplankton-Detritus (NPZD) model. In the study, we have considered cyclone Hudhud (category-4), which passed over a cyclonic eddy in the BoB during 7-12 October 2014. Before the passage of cyclone Hudhud, strong stratification in the upper ocean inhibited eddy-driven upwelling of nutrients to the mixed layer and limited the phytoplankton production. However, when cyclone Hudhud interacted with the cyclonic eddy, which further reduced the water column stability (one order less) of the upper ocean and initiated the wind-driven upwelling. This mechanism resulted in the easy upwelling of cold nutrient-rich water to the mixed layer. A case study presented here demonstrates ocean-atmosphere (eddy-cyclone) interaction and its influence on the mixed layer Chl_a production in the northern BoB. Our study showed that column integrated Chl_a value in the upper 100 m increased by 70 % when cyclone Hudhud passed over a cyclonic eddy region in the BoB. The present study suggested that cyclonic eddy accompanied by cyclone Hudhud induced the Chl_a bloom in the Northern Bay during the post-monsoon season of 2014.

Keywords: Bay of Bengal, Biogeochemical model, Cyclonic eddy, Cyclone, Stratification

Key Points

- Stratification inhibits eddy-driven upwelling in the northern Bay of Bengal.
- Eddy-cyclone interaction reduces the water column stability and initiates upwelling in the Bay of Bengal.
- Eddy-cyclone interaction induced phytoplankton bloom in the Bay of Bengal.

1. Introduction

The Bay of Bengal (BoB) is a tropical semi-enclosed basin located in the eastern part of the north Indian Ocean (Figure 1). The BoB is bordered by India, Sri Lanka, Bangladesh, Myanmar and Andaman-Nicobar Islands. The basin experiences dominant semi-annually reversing monsoon winds blowing from the southwest during summer (June-September) and northeast during winter (December-March). A large amount of riverine influx ($2.5 \times 10^{12} \text{ m}^3 \text{ y}^{-1}$) and excess precipitation over evaporation make the northern BoB region highly stratified (Schott & McCreary, 2001). The strong stratification during the summer (Rao & Sivakumar, 2003) causes the formation of the barrier layer (the layer between the base of the mixed layer and the top of the thermocline) in the northern bay. It does not allow the prevailing winds to break the stratification. This, in turn, inhibits the upwelling of nutrients from the deep layer to the euphotic zone. The above-said characteristics make the BoB highly oligotrophic during the summer and post-monsoon season (Prasanna Kumar et al., 2002), except during the events of mesoscale eddies (Prasanna Kumar et al., 2004) and tropical cyclones (Vidya et al., 2017). In BoB, mesoscale eddies are ubiquitous (Prasanna Kumar et al., 2004), while tropical cyclones occur only during the post and pre-monsoon seasons with maximum frequency during the post-monsoon season (Neetu et al., 2012).

Tropical cyclones bring nutrient-rich subsurface water to the surface and stimulate phytoplankton growth (Eppley & Renger, 1988). Passage of cyclone initiates the upper ocean mixing, leading to a decrease in sea surface temperature (SST) and alter the upper ocean primary production. The main properties that a cyclone could modify are mixed layer depth, thermocline depth and air-sea heat fluxes (Sun et al., 2014). Price (1981) showed that entrainment and upwelling are the two major physical processes that bring up the nutrient-rich water to the upper euphotic zone and stimulate biological production. Earlier studies (e.g., Babin et al., 2004; Tummala et al., 2009; Vidya et al., 2017; Vinayachandran & Mathew, 2003) showed increased phytoplankton biomass (Chl a) in the BoB after the passage of a cyclone. Furthermore, BoB contains many cyclonic eddies, which also contribute to the increase of phytoplankton biomass (Prasanna Kumar et al., 2004; Prasanna Kumar et al., 2007; Vidya & Prasanna Kumar, 2013). Most of the time, cyclones pass over the cold/warm-core eddies in the BoB as there are many eddies in BoB throughout the year (Prasanna Kumar et al., 2002).

Eddy – cyclone interactions have been a poorly studied scientific topic as far as the Indian Ocean is concerned. Pre-existing cyclonic eddy can intensify the cooling processes along the cyclone's track and shallow the mixed layer depth (Liu et al., 2009). Liu & Tang (2018) showed that typhoon in the South China Sea strengthened the pre-existing cyclonic eddy and intensified the

phytoplankton bloom. Their study demonstrated that when a typhoon passed over a cyclonic eddy region, the chlorophyll-a (Chl a) increased by approximately 35%. In contrast, when it passed over a non-eddy region, the Chl a enhancement was only 12%. Previous studies (Liu et al., 2009; Maneesha et al., 2011; Patnaik et al., 2014; Sadharam et al., 2012; Sun et al., 2014; Zheng et al., 2008) have shown that pre-existing eddy such as anti-cyclonic (warm-core) and cyclonic (cold-core), played a significant role in determining the strength and location of large SST cooling. Using satellite-derived data and numerical simulations, few studies (Anandh et al., 2020; Gordon et al., 2017; Patnaik et al., 2014; Vidya et al., 2017) highlighted the importance of interaction between oceanic eddies and tropical cyclones in the BoB. Using an ocean-atmosphere coupled model, Anandh et al. (2020) and Patnaik et al. (2014) showed that when a cyclone passed over the eddy, it gets intensified in the BoB. Gordon et al. (2017) showed that rapid intensification and transformation of anticyclonic eddy occurred in the BoB after the passage of a tropical cyclone using observational data. All the above studies highlighted that eddies play an important role in the intensification and dissipation of BoB cyclones. Using satellite-derived Chl a , Vidya et al. (2017) showed that passage of tropical cyclone Phailin (Category 5; 8-14 October 2014) over the cold-core eddy (in the northern BoB) caused the intensification of pre-existing eddies and thus resulted two times enhancement in Chl a after the cyclone passage. Though the prevailing winds were strong over the region, the strong stratification in the region inhibits the upwelling and thus led to the less entrainment of nutrient to the surface, which subsequently affected the Chl a production. Since eddy and tropical cyclone co-occur, none of the above studies explored the role of individual processes towards the Chl a /phytoplankton production in the BoB during post monsoon season.

The present study explores how the pre-existing cyclonic eddy affected the upper ocean processes when the cyclone Hudhud passed over the northern BoB during 07-12 October 2014. As the cyclone and cyclonic eddy were co-occurring, it is not possible to quantify the role of individual processes towards the Chl a /phytoplankton production using *in situ* and satellite data. The best way to achieve this scientific question is to address it through the help of a numerical model. In the present study, two numerical simulations (Experiment I and II) were carried out to investigate the importance of the pre-existing cyclonic eddy in the event of cyclone Hudhud and its impact on the Chl a /phytoplankton production in the BoB.

2. Data and Methods

2.1 Cyclone Hudhud

The National Oceanic and Atmospheric Administration hurricane forecasters and World Meteorological Organization use the Saffir-Simpson category scale (1–5 based on the cyclone/hurricane intensity at the indicated time) (Simpson, 1974), which assigns storms (cyclones) to five categories (<https://www.nhc.noaa.gov/aboutsshws.php>). Cyclone ‘Hudhud’ is a category- 4 cyclone (as per the Saffir-Simpson category scale) developed in the BoB during 7-14 October 2014 (Figure 1). It originated as a low-pressure area over the Tenasserim coast and adjoining the North Andaman Sea on 6th October 2014. It concentrated into a Depression on 7th October 2014 over the North Andaman Sea. On 8th October, it emerged into Southeast BoB and continued to move west-northwestwards, then intensified into a Severe Cyclonic Storm (SCS) on 09th October. It further developed as a Very Severe Cyclonic Storm (VSCS) in the afternoon of 10th October 2014 (category 1). It continued to intensify while moving northwestwards and reached maximum intensity in the early morning of 12th October 2014 with a maximum sustained wind speed of 180 kmph (category-4) over the west-central BoB off the Andhra Pradesh coast, India. It crossed the north Andhra Pradesh coast over Visakhapatnam between 1200 and 1300 hrs IST of 12th October 2014 with the same wind speed (<http://www.rsmcnewdelhi.imd.gov.in/images/pdf/archive/bulletins/2013/RHUD.pdf>).

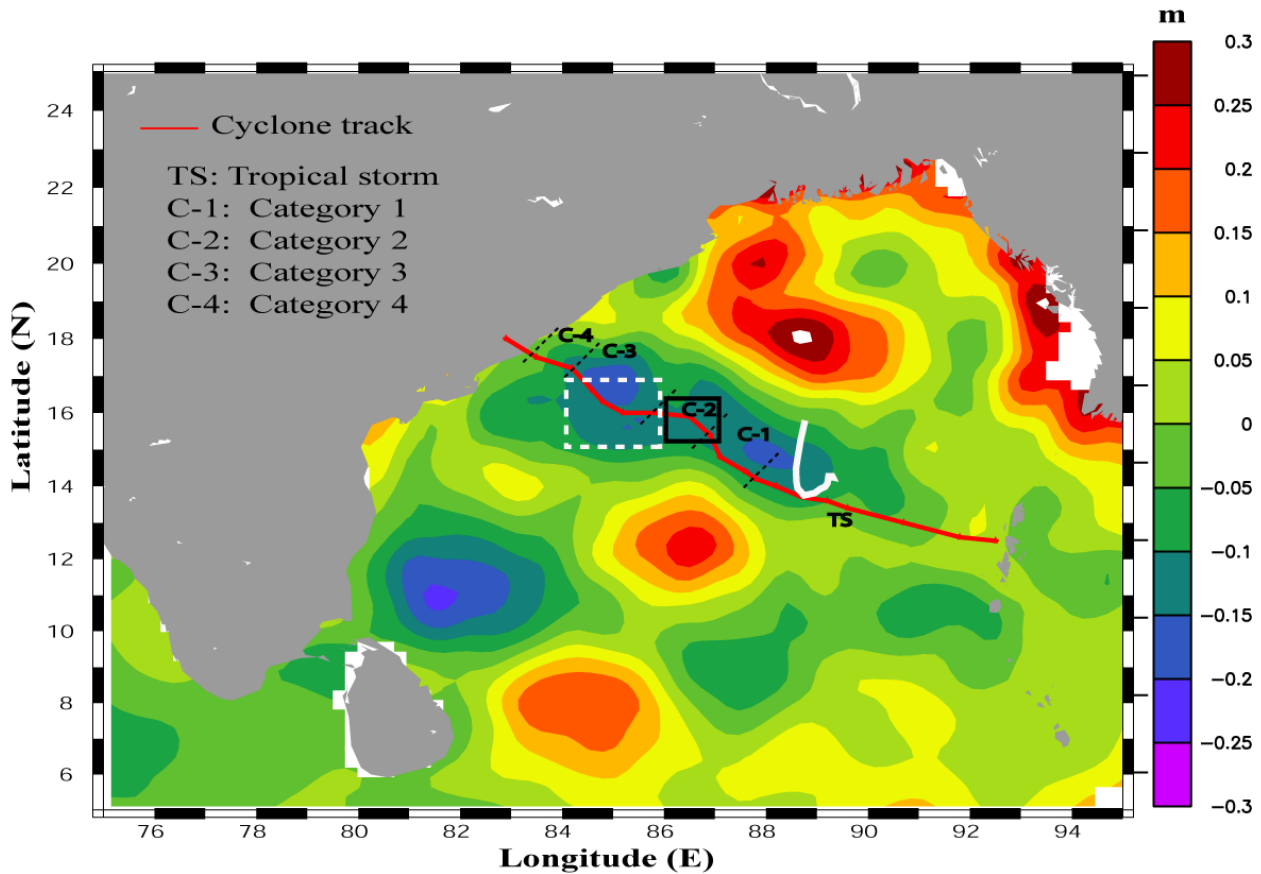


Figure 1. Satellite-derived sea surface height anomaly during 07-12 October 2014. The red line represents the track of cyclone Hudhud with an interval of every six hours (The classification is based on the Saffir-Simpson category scale; C1- category 1, C2-category 2, C3- category 3 and C4- category 4), dashed white rectangle ($84\text{-}86^{\circ}\text{E}$ and $15\text{-}17^{\circ}\text{N}$) indicates the region chosen for further study, the black dashed slanting lines indicate the boundary of different category cyclone. The thick white line indicates the location of Argo float (WMO ID- ID- 2902114). The thick black box indicates the Chla in the non-eddy region shown in Figure S12.

2.2 Satellite data

Chla concentration and sea surface height anomaly

The Chla concentration data from version 3.1 (v3.1) of the European Space Agency's Ocean Color Climate Change Initiative (OC-CCI) with a spatial resolution of 4 km and temporal resolution of 8 days was used. The OC-CCI Chla product (Sathyendranath et al., 2018) is made up of globally merged MERIS, Aqua-MODIS, SeaWiFS and VIIRS data (source: <http://www.esa-oceancolour-cci.org/>). Sea level observations from the satellite altimetry can be used to detect mesoscale features. The spatial structure of the cyclonic eddy was examined by analyzing daily snap-shots of merged sea-level anomalies from all altimeter missions (Jason-3, Sentinel-3A, HY-2A, Saral/AltiKa, Cryosat-2, Jason-2, Jason-1, T/P, ENVISAT, GFO, ERS1/2). The satellite altimetry product was generated by the Sea Level Thematic Assembly Center (SL-TAC) and distributed by the Copernicus Marine and Environment Monitoring Service (CMEMS, <http://marine.copernicus.eu/>). We used the

delayed time mode sea level anomaly data (product ID: SEALEVEL_GLO_PHY_L4_REP_OBSERVATIONS_008_047) with a spatial resolution of $0.25^\circ \times 0.25^\circ$ and temporal resolution of 1 day.

2.3 Model description and numerical experiments

2.3.1 Physical model

The present study employed the Regional Ocean Modeling System (ROMS), which is a free-surface, split-explicit and 3-dimensional primitive equations oceanic model. ROMS utilises a non-linear terrain-following coordinate (Shchepetkin & McWilliams, 2005). It employs short time steps to advance the surface elevation and barotropic momentum equations. It uses a much larger time step for temperature, salinity, and baroclinic momentum. A third-order accurate predictor (Leap-Frog) and corrector (Adams-Molton) time-stepping algorithm is used for time discretization. The vertical discretization in the model follows the stretched terrain-following coordinates, which allows high resolution in the mixed ocean layer and bottom boundary layer suitable for different applications. The horizontal grid staggering in the ROMS model is based on Arakawa C-grid. ROMS allows vertical and horizontal advection schemes and parameterization for vertical and horizontal mixing. The ROMS (version 3.7) model domain configuration is shown in Figure 2. The model configured in the present study has a higher horizontal resolution of 1/12-degree (9 km), which explicitly resolves eddy, including mesoscale processes. It has time step of 60s and 40 vertical sigma levels (increased resolution near the surface and bottom), with vertical stretching parameters such as bottom stretching parameter (θ_b)=0.4, surface stretching parameter (θ_s)=7, and vertical s coordinate parameter (HC)=10m. The southern and western boundary is open while the northern and eastern are closed. The open boundary conditions are applied to tracers and baroclinic velocity using a combination of radiation conditions and nudging (Chen et al., 2013; Marchesiello et al., 2001) to daily temperature and salinity fields from the latest version of Climate Forecast Systems (CFSv2) operational analyses developed in National Centers for Environmental Prediction (NCEP) (Saha et al., 2014). A Flather boundary condition (Flather, 1975) was applied for the barotropic currents that enable free propagation of wind-generated currents and tides in the open boundaries. Generic Length Scale scheme (Umlauf & Burchard, 2003) is used for the vertical mixing parameterization with ' ω ' closure proposed by (Warner et al., 2005). The overview of the ROMS model configuration is presented in Table S1.

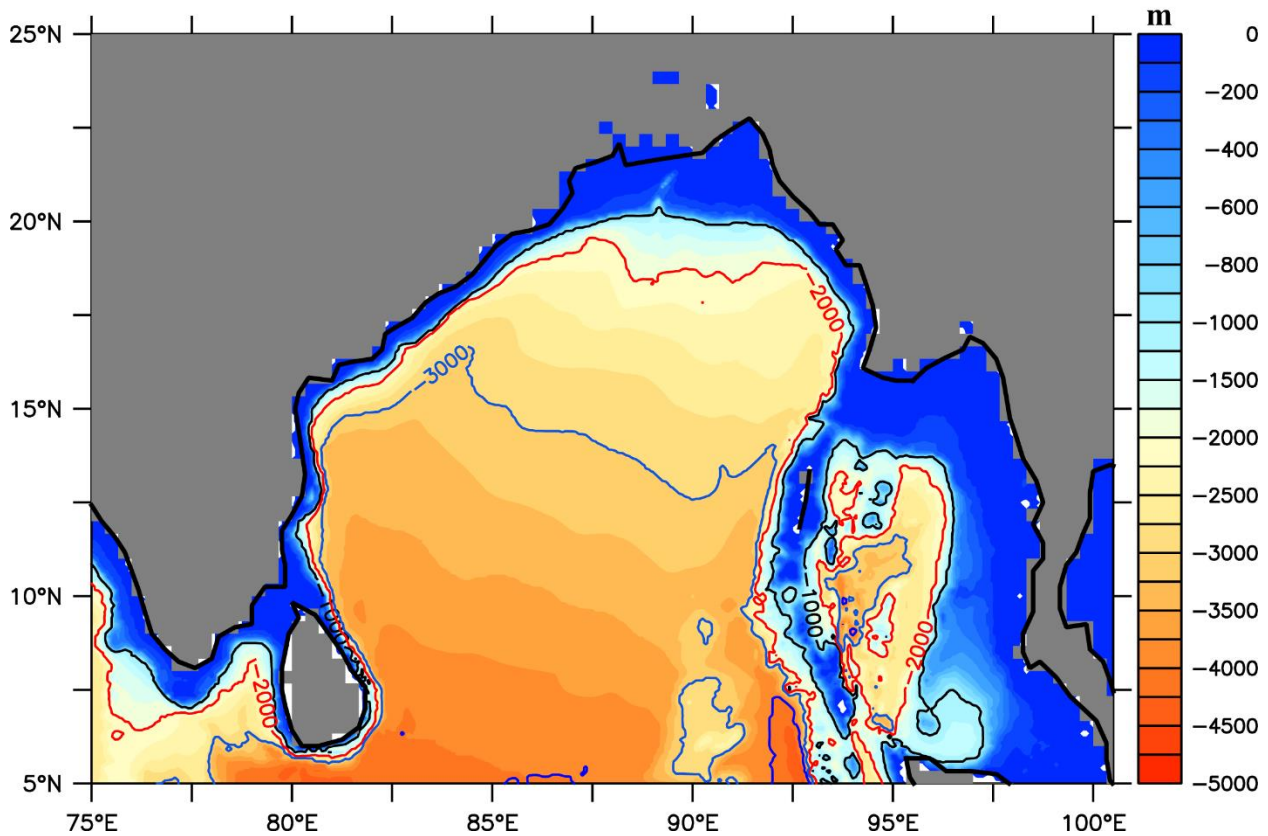


Figure 2: The domain of ROMS model configuration (Bay of Bengal) with its bathymetry (in m). Black contour indicates 1000 m, red contour indicates 2000 m, and blue contour indicates 3000 m.

2.3.2 NCEP-CFSv2

The ocean initial and boundary conditions, atmospheric forcing conditions for ROMS were derived from the latest version of Climate Forecast System (CFSv2) operational analyses developed in the National Centers for Environmental Prediction (NCEP). CFSv2 is the state-of-art, fully coupled climate forecast system model that became operational in August 2011 (Saha et al., 2014a). CFSv2 has undergone a substantial upgrade in the forecast system compared to CFSv1, mainly through model components and data assimilation system. This includes a) the incorporation of 3 layers interactive global sea ice model and global land data assimilation, b) upgrade of ocean model to MOM4, and c) upgrade of the land surface model to 4-layer NOAH land model. Many modeling studies have reported the potential improvement in climate forecast system CFSv2 through extensive evaluation studies (Yuan et al., 2011; Kim et al., 2012; Barnston and Tippett, 2013; Zuo et al., 2013; Goswami et al., 2014; Pokhrel et al., 2012). The six-hourly CFSv2 atmosphere and ocean analyses have a 0.5° spatial resolution with 38 and 40 vertical levels, respectively.

The ROMS (stand-alone) model is spun up for ten years to attain the mean ocean properties and circulation features using temperature (Locarnini et al., 2013) and salinity (Zweng et al., 2013) fields obtained from World Ocean Atlas (WOA 2013), which is referred as climatology run. The

model solutions obtained from the climatology run is used to perform two ROMS-biogeochemical experiments as described below:

2.3.3 Biological model

The details of the biological component of the model, such as schematic, equations and parameters of the model, are given in Fennel et al. (2006, 2008, and 2011). The Nutrient-Phytoplankton-Zooplankton-Detritus (NPZD) model is a nitrogen-based model with seven state variables. It consists of two species of dissolved inorganic nitrogen (nitrate and ammonium), phytoplankton group (Phy), chlorophyll *a* (Chl_a), zooplankton group (Zoo), and two pools of detritus (Large Detritus-LDet and Small detritus-SDet). The biological variables NH₄, Phy, Chl, Zoo, SDet and LDet, were initialized with small constant values. All the biological state variables at the boundary are set to small positive values (K. Fennel et al., 2011).

2.3.4 Numerical Experiments

ROMS coupled with an established NPZD - type planktonic ecosystem-biogeochemistry model that is described in Katja Fennel et al. (2006; 2008) and was simulated from 00 UTC of 01st January 2014 to 18 UTC of 30th October 2014. The initial ocean conditions, boundary conditions, and atmospheric surface forcing fields were derived from NCEP-Climate System Version 2 (CFSv2) analysis at six hourly intervals. The initial and boundary conditions for oxygen and nitrogen were derived from WOA 2013, whereas Chl_a was obtained from the monthly mean Sea-viewing Wide Field-of-view Sensor (SeaWiFS). The ocean model was simulated for ten years using climatological forcing and boundary conditions. For the realistic experiment, both experiments (Experiment 1 and Experiment II) were initialized with initial ocean conditions based on climatology simulation corresponding to January (average of last seven years), atmospheric forcing data based on NCEP CSFR and biogeochemical inputs based on WOA13 and SeaWiFS monthly climatology. Vertical profiles of Chl_a from satellite data for model initialisation was computed based on Morel and Berthon (1989). The details of the two experiments used in the present study are given below.

Experiment I

This experiment was based on climatological wind stress forcing, which aimed to reproduce the primary productivity contributed only by the pre-existing cyclonic eddy. The model configuration was the same as the Experiment II (see below paragraph), with the exception of the atmospheric surface winds that were acquired from climatological winds that do not include the Hudhud cyclone winds (Wind stress was computed from wind speeds shown in Figure 3; black line).

Experiment II

This experiment was based on realistic wind stress forcing using NCEP-CFSv2 (Wind stress was computed from wind speeds shown in Figure 3; red line), which enables the investigation of the eddy-cyclone interaction in the BoB i.e., the combined eddy and cyclone contribution to the observed primary productivity.

2.3.4 Equations used

The ocean stratification (Brunt Vaisala frequency) in the upper 100 m water column was calculated using the temperature and salinity data from the model.

$$N = \sqrt{\frac{g}{\rho} \frac{\partial \rho}{\partial z}} \quad (1)$$

The frequency (N) quantifies the importance of stability (s^{-1}), 'ρ' is the density ($kg\ m^{-3}$) of the water, and 'z' is the depth (m).

The time evolution of the vorticity gradients is determined by using the Okubo-Weiss (Okubo, 1970, Weiss, 1981) parameter (OW),

$$ow = S_n^2 + S_s^2 - \omega^2, \quad (2)$$

Where S_n , S_s and ω are the normal and shear components of strain and the relative vorticity of the flow defined respectively by

$$S_n = \frac{\partial u}{\partial x} - \frac{\partial v}{\partial y}, \quad S_s = \frac{\partial v}{\partial x} + \frac{\partial u}{\partial y}, \quad \omega = \frac{\partial v}{\partial x} - \frac{\partial u}{\partial y}. \quad (3)$$

The parameter OW allows separating the flow into a vorticity-dominated region (negative value) and a strain-dominated region (positive value).

The mixed layer salinity budget in the ocean is mainly influenced by oceanic advection, diffusion, entrainment, and air-sea freshwater flux (evaporation minus precipitation) and computed using the equation followed by Dong et al. (2009) as below,

$$\frac{\partial S_m}{\partial t} = \frac{S_m(E-P)}{h_m} - u_m \nabla S_m + \kappa \nabla^2 S_m - \frac{w_e \Delta S}{h_m} \quad (4)$$

Where S_m is the mixed layer salinity, h_m is the mixed layer depth, w_e is the entrainment velocity, ΔS is the salinity difference between the mixed layer and just below the mixed layer, and k is the eddy diffusivity (taken as $500 \text{ m}^2 \text{ s}^{-1}$). E and P represent the evaporation and precipitation rates, respectively. Similarly, the mixed layer nitrate budget was computed using the equation followed by Resplandy et al. (2011).

This study intends to explore how the pre-existing cyclonic eddy affected the upper ocean processes when cyclone Hudhud passed over the northern BoB region. Hence, we selected a region $84\text{-}86^\circ\text{E}$ and $15\text{-}17^\circ\text{N}$ (white dashed rectangle in Figure 1), where both cyclonic eddy and cyclone Hudhud co-exist. For further analysis, we have used physical and biological data averaged over the same region.

3. Results and Discussions

3.1 Physical Response

Figure 1 represents the track of cyclone Hudhud in the BoB. The cyclone Hudhud is represented as TS (tropical storm), C1(category 1), C2 (category 2), C3 (category 3) and C4 (category 4), respectively, according to the Saffir-Simpson scale. Negative sea level anomaly (SLA) along the cyclone track confirmed the presence of cyclonic eddy (Figure 1) in the region. In this study, we carried out two experiments. The first experiment used the climatological winds/ stress (Figure 3; black line), and the second experiment used cyclone winds/stress (Figure 3; red line). Experiment I gives the details of processes contributed by cyclonic eddy, whereas Experiment II provides the combined effect of cyclonic eddy and cyclone Hudhud. Along the cyclone track, wind speed in Experiment I was 1 m s^{-1} (black line, Figure 3), while in Experiment II, it varied from $18\text{-}65 \text{ m s}^{-1}$ (red line, Figure 3).

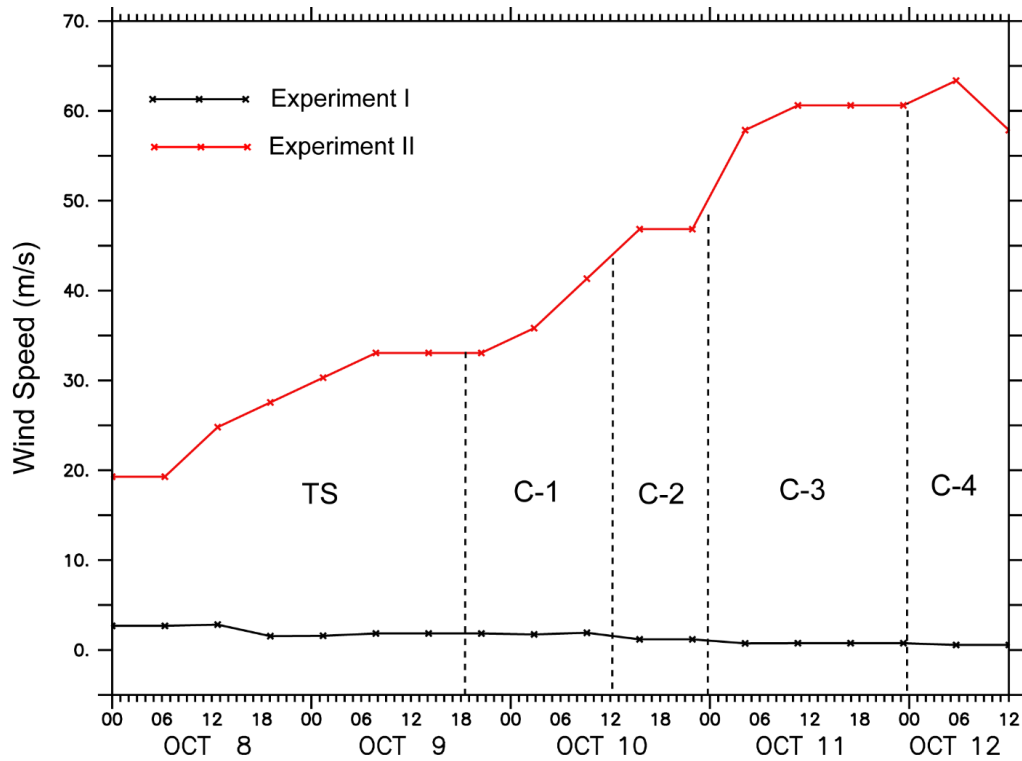


Figure 3. Wind speed (model is forced with wind stress) along the cyclone track in Experiment I (black line; only cyclonic eddy present) and Experiment II (red line; co-occurrence of cyclonic eddy and cyclone Hudhud).

In the BoB, mesoscale eddies radius range from 50-150 km, and their life span varies from a few weeks to months (Chen et al., 2012). Our model is an eddy-resolving model with a horizontal resolution of 9 km. We believe that this model can simulate the BoB eddies (radius ranging from 50-150 km) and associated phytoplankton dynamics. To understand the spatial variability of the eddy structure and the ability of the model to reproduce the mesoscale eddy, we have plotted depth of 26°C isotherm (d26) overlaid with the currents in the upper 100 m water column (vectors are averaged over the top 100 m water column) on 08th October 2014 (first day of the cyclone formation) and 18th October 2014 (after the cyclone) respectively (Figure 4a & 4c). We also compared model surface currents with the Ocean Surface Currents Analyses Real-time (OSCAR) data before the cyclone (on 6th October 2014) (Figure S1). Closed contours in the study region (red rectangle) in Figure S1 a and b confirm that model can reproduce the cyclonic eddy in the study region before the cyclone. Tropical cyclones develop over the warm oceans, more specifically above the surface temperature above 26°C. Hence, tropical cyclone heat potential is defined as a measure of the integrated vertical temperature from the sea surface to depth of the 26°C isotherm (Goni et al., 2013). The shallow d26 along with anticlockwise current (vector) direction represent the eddy-driven upwelling in the region. Besides, we also computed the Okubo-Weiss (OW) parameter on those days

(8th and 18th October 2014) using the data from model simulated currents (Figure 4b & 4d). Eddies are seen as closed contours which enclose the region of large negative OW (Figure 4b & 4d). The OW during the Experiment I and II are shown in Figure S2. In addition, we also compared spatial maps of SST and SLA from model and satellite, which is shown in Figure S3 and S4, respectively. Kindly note that the reference level of the Aviso SSHA and ROMS free surface is different (Zhou Chaojie et al., 2018). This may cause some changes in SSHA when we compare model SSHA with satellite-derived SSHA (Figure S4). The above analysis (Figure 4 & S1-S4) further confirmed that the model could simulate/capture the mesoscale eddies in the BoB. A similar figure which depicts the d26 and OW during the cyclone periods (11th and 14th October 2014) is given in Figure S5. Shoaling of d26 (Figure 4b), more negative OW parameter (Figure 4d) and dropping of sea surface height anomaly from -7 cm to -14 cm (Figure 5) when cyclone enters the eddy region indicated the intensification of the cyclonic eddy after the passage of cyclone Hudhud.

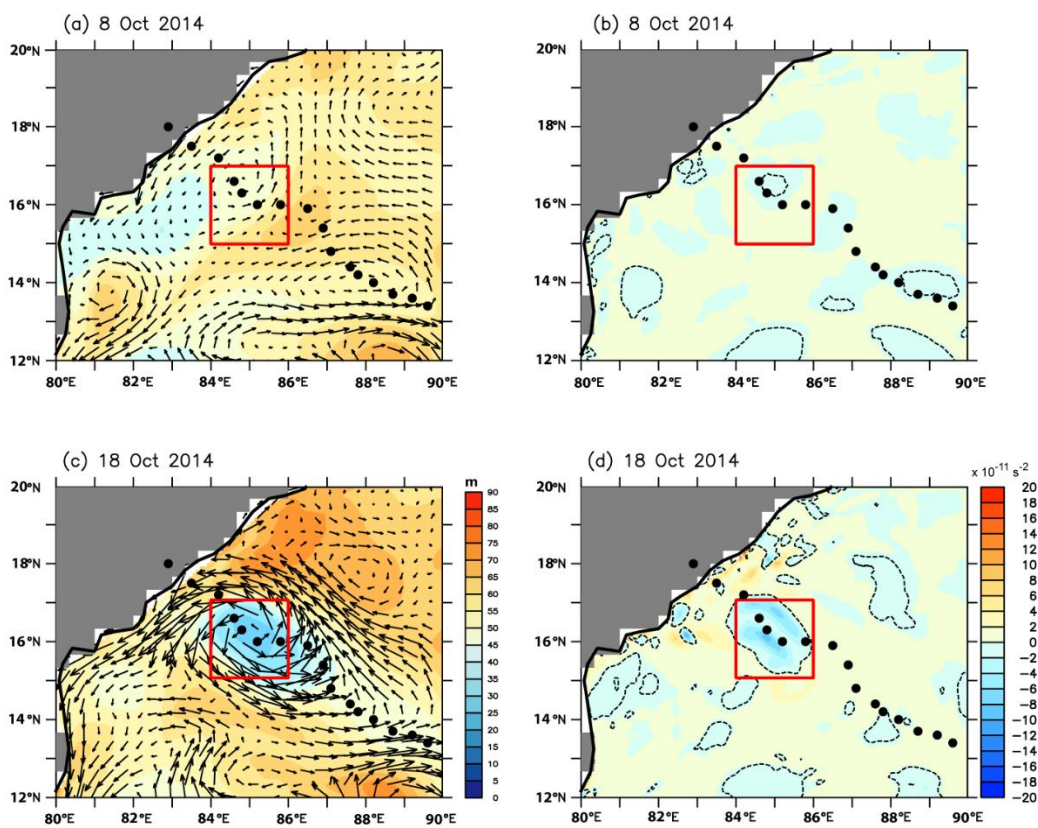


Figure 4. The spatial pattern of the depth of 26-degree isotherm overlaid with currents in the upper 100 m from the model (a) before and (c) after cyclone Hudhud. Okubo-Weiss parameter computed from the model currents in the upper 100 m (b) before and (d) after the cyclone. The red rectangle represents the region where cyclone and eddy co-exist.

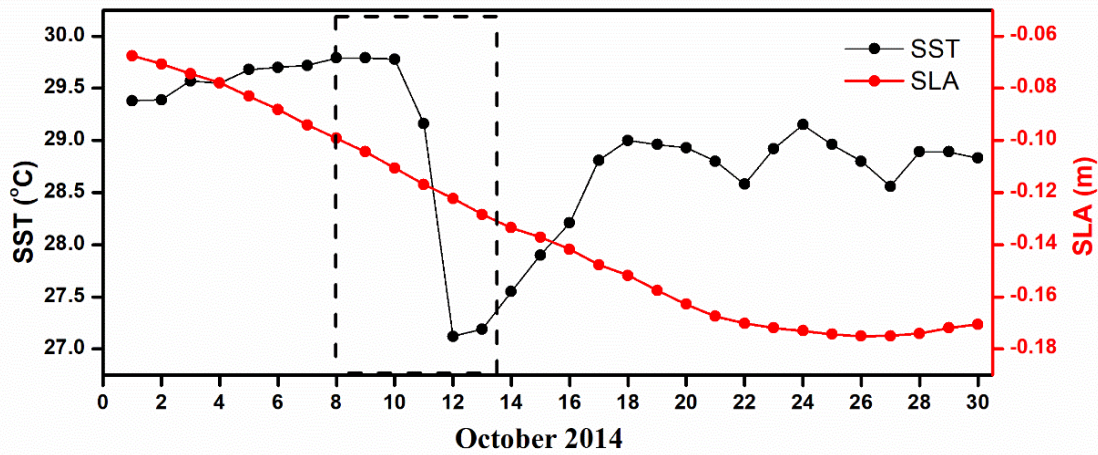


Figure 5. Time series of SST (black line) and sea level anomaly (SLA; red line) averaged over the region 84-86°E and 15-17°N.

We also analyzed SST and SLA in the region (averaged over the region 84-86°E and 15-17°N), where eddy-cyclone co-occur (Figure 5) to explore the oceanic variations associated with cyclone Hudhud. As SST is generally considered as a criterion for oceanic cooling in response to the cyclone passage, we analyzed SST (Figure 5; black line) and SLA (Figure 5; SLA: red line). Note that SST cooling of ~2.5 °C was observed on 12th October 2014 when cyclone entered the eddy region. However, SST resumed its warming trend from 13th onwards. Similar to SST, the magnitude of the SLA increased from -7 cm to -14 cm (Figure 5; red line) when cyclone entered the eddy region. We further analysed the upper ocean parameters such as water column temperature, salinity and stability in the two experiments to understand the upper ocean characteristics of the region.

Vertical sections of temperature, salinity and water column stability (averaged over 84-86°E and 15-17°N) during Experiment I and II are shown in Figure 6 (a – f). The rain rate used as an input forcings in both the experiment averaged over the same region (Figure 6g). In Experiment I, the vertical structure of temperature showed a stratified water column in the upper 100 m (Figure 6a), while 27°C isotherm shoaled from 50 m to the surface during the cyclone period in Experiment II (Figure 6b). In the absence of cyclone winds (Experiment I), the isotherms are deeper (Figure 6a). Vertical salinity structure consists of freshwater in the upper 20 m, indicating the stratified water column in Experiment I (Figure 6c). However, isohalines shoaled and reached upto the surface in Experiment II (Figure 6d). Water column stability (also called as Brunt-Vaisala frequency which represents the intensity of the stratification of the water column) showed more positive values (~0.34 s⁻¹) in the upper 20 m in Experiment I (Figure 6e) compared to Experiment II. One order less magnitude (0.06 s⁻¹, Figure 6f) in Brunt Vaisala frequency in Experiment II during the cyclone

period (11th October 2014) indicated that the water column was more stable and stratified in Experiment I compared to Experiment II. To understand the difference in salinity between the two experiments, we compared the spatial distribution of surface salinity overlaid with currents (Figure S6). Surface salinity showed different patterns in both experiments, which indicated different ocean circulation (Figure S6). Though we used the same forcings in both the experiments, only winds/wind stress were different. We believe that the difference in salinity in the upper 20 m (Experiment I) is contributed by intense rainfall (Figure 6g) during the cyclone period. However, the strong winds ($> 60 \text{ m s}^{-1}$) in Experiment II created vertical shear and caused upwelling or entrainment, whereas winds were much weaker in experiment I ($\sim 1 \text{ m s}^{-1}$). The individual role of upwelling and entrainment processes during the cyclone period was quantified using the mixed layer budget analysis of salinity followed by Dong et al. (2009). Since our interest was to explore the relative importance of upwelling and entrainment, only those two terms are shown in Figure 7 along with MLD variation (Figure 7; black line). The upwelling term showed positive values on 11th and 12th October 2014 (Figure 7; filled red circle), while the entrainment term showed values close to zero (Figure 7; red circle). The above analysis indicated that the strong winds/wind stress during the cyclone period broke the salinity driven stratification and initiated upwelling of cold water to the surface. After exploring the physical processes, it was further analysed for the Chl*a*/phytoplankton responses from the two different experiments.

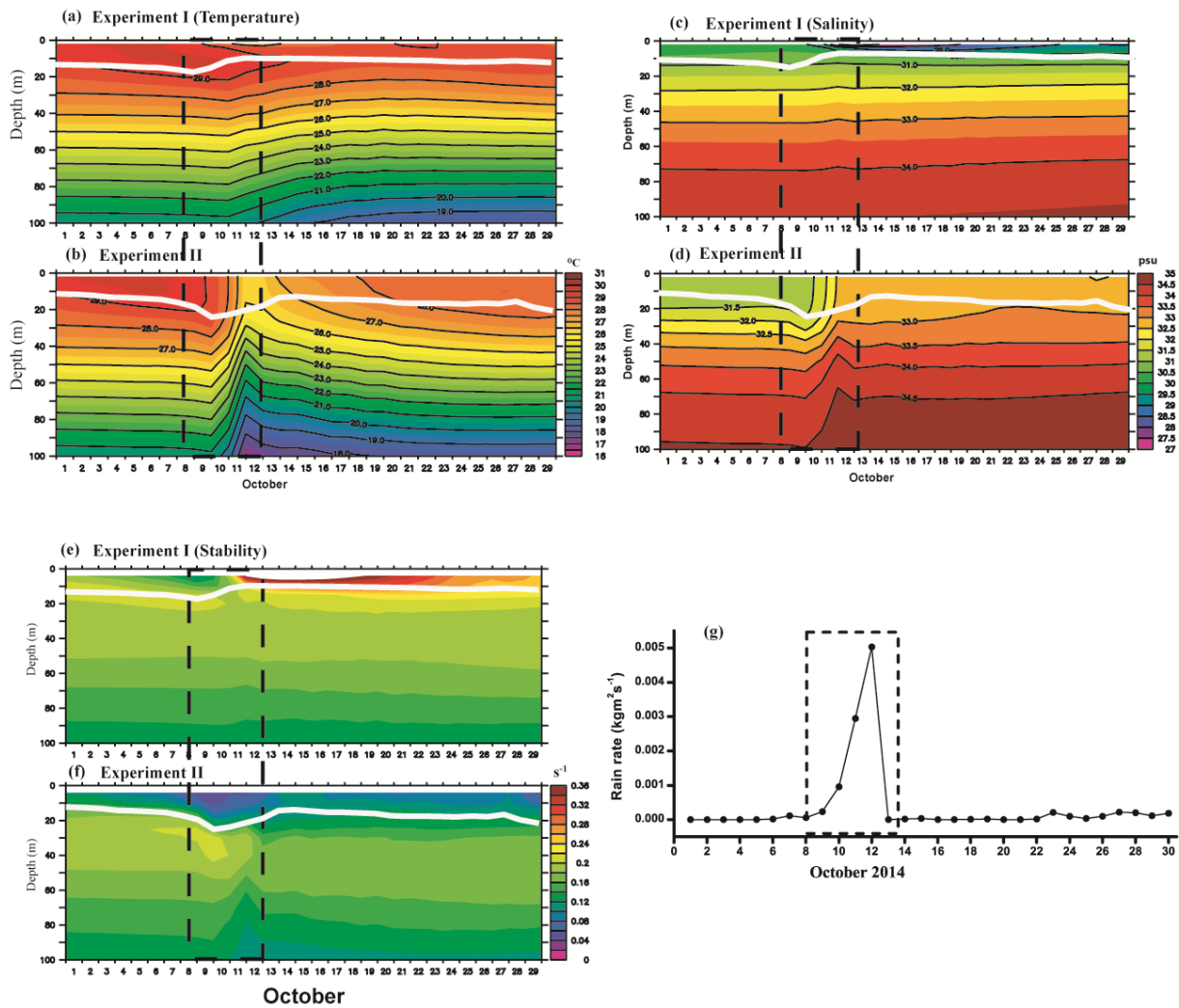


Figure 6. Time series of vertical structure [averaged over the region 84-86°E and 15-17°N] of temperature in (a) Experiment I and (b) Experiment II. Vertical structure of salinity in (c) Experiment I and (d) Experiment II. Vertical structure of water column stability (Brunt Vaisala frequency in s⁻¹) in (e) Experiment I and (f) Experiment II. (g) Time series of rain rate used as input forcing in the model. The Black dashed rectangle represents the cyclone period. The white contour in figures a-f indicates MLD.

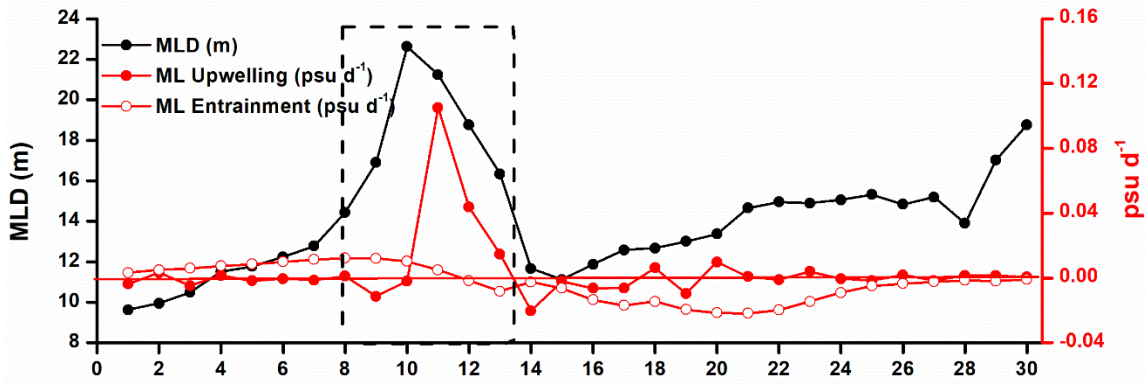


Figure 7. Time series of mixed layer depth (MLD; black line), upwelling term (red filled circle) and entrainment term (red circle) computed using mixed layer salinity budget.

3.2 Biological Responses

Chl*a* concentration-response from the satellite and model

The satellite and model-derived surface Chl*a* concentration before (phase 1), during (phase 2) and after (phase 3) the cyclone is shown in Figure 8 (a-f). The average Chl*a* concentration before the cyclone was $< 0.2 \text{ mg m}^{-3}$, while after the passage of cyclone Hudhud, the Chl*a* concentration increased up to approximately 3 mg m^{-3} . The white patches during the cyclone in figure 8a indicate the absence of satellite-based Chl*a* concentration data. The strong cloud cover during the cyclone does not permit the satellite to capture the Chl*a* concentration during its passage. However, the model can capture Chl*a* concentration during the cyclone, which is an added advantage of the numerical modeling technique.

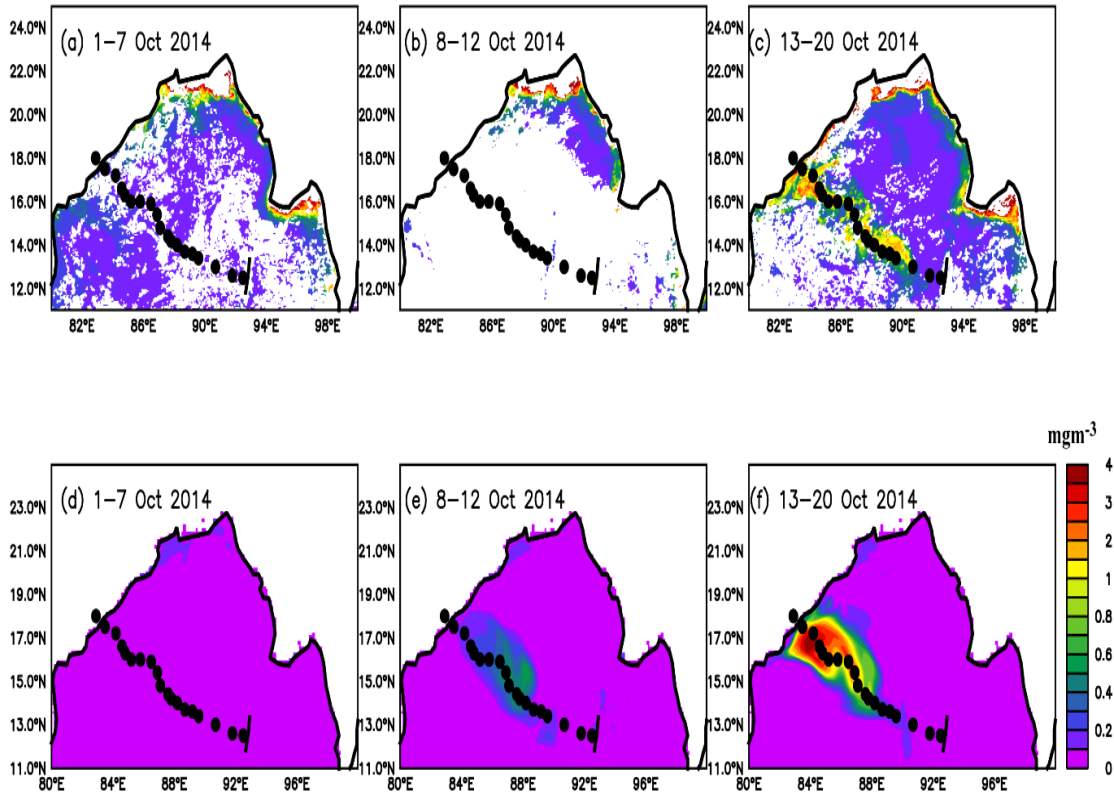


Figure 8. Chla concentration in mg m^{-3} from the (a-c) satellite (a, Phase 1; b, phase 2 and c, phase 3) and (d-f) model (d, phase 1; e, phase 2 and f, phase 3).

We further analysed the time series of the vertical structure of Chla concentration in the upper 100 m (including subsurface Chla) in both the experiments (Figure 9 a & b). In addition, we also compared the vertical structure of Chla obtained from the Argo float (WMO ID- 2902114; thick white line in Figure 1), which was located in the cyclone track (Figure S7) with that of the model. The above analysis (Figure 9b and Figure S7) confirmed that the model could simulate/capture surface and subsurface Chla maxima well in the BoB. In Experiment I, Chla showed the subsurface maxima at ~ 70 m with the oligotrophic upper ocean during phase 2 and phase 3 (Figure 9a). As the nitracline was below the MLD in all three stages, it did not allow to form the Chla bloom in Experiment I after the cyclone. However, in Experiment II, the strong wind stress resulted the upwelling of nitracline to the mixed layer, which subsequently increased the Chla from 0.2 mg m^{-3} to 2.5 mg m^{-3} at the surface and from 3 mg m^{-3} to 4.5 mg m^{-3} at subsurface (Figure 9b). We also computed column integrated Chla, which increased from 82.5 mg m^{-2} to 140 mg m^{-2} and indicated a 77 % increase in the Chla production after the cyclone (Figure S8; blue line).

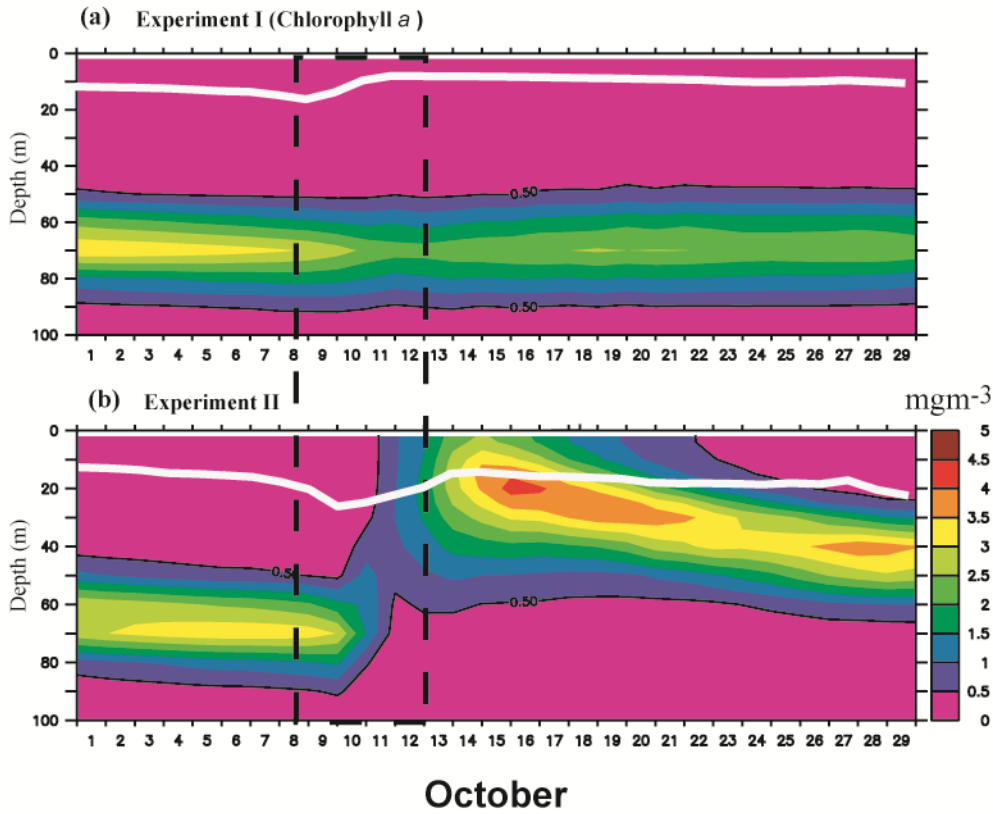


Figure 9. Time series of the vertical structure of Chla (in mg m^{-3} ; averaged over the region $84\text{-}86^\circ\text{E}$ and $15\text{-}17^\circ\text{N}$) in (a) Experiment I and (b) Experiment II. White contours indicate MLD. Black contours indicate 0.5 mg m^{-3} Chla. The black dashed rectangle represents the cyclone period.

Oceanic processes/factors like mixed layer depth (MLD), barrier layer thickness (BLT), and nitracline depth can modulate the Chla concentration in the ocean. It is explored how the above factors influence the Chla concentration after the passage of cyclone Hudhud. MLD is defined as the depth at which the density is 0.2 kg m^{-3} higher than the surface value. BLT is the difference between the Isothermal Layer Depth (ILD) and MLD. ILD is computed using the depth at which temperature decreases by 0.8 degree from SST (Kara et al., 2000). The presence of a thicker barrier layer indicates a more stable water column, and more difficult for the cyclone to mix the upper ocean. Nitracline is an ocean layer in which nitrate level increases rapidly with depth. We used a depth of 1 mmol m^{-3} nitrate isocline to define the nitracline (Figure 10, white contour). Figure 10 represents the time series of the vertical structure of nitrate in the upper 100 m overlaid with nitracline, MLD (back contours) and BLT (red contours). Note that all the time series were computed by averaging over the region $84\text{-}86^\circ\text{E}$ and $15\text{-}17^\circ\text{N}$ (shown as a dashed white rectangle in Figure 1). We also computed MLD, BLT and ILD from the Argo float, which was fortunately located in the cyclone track (Figure S10).

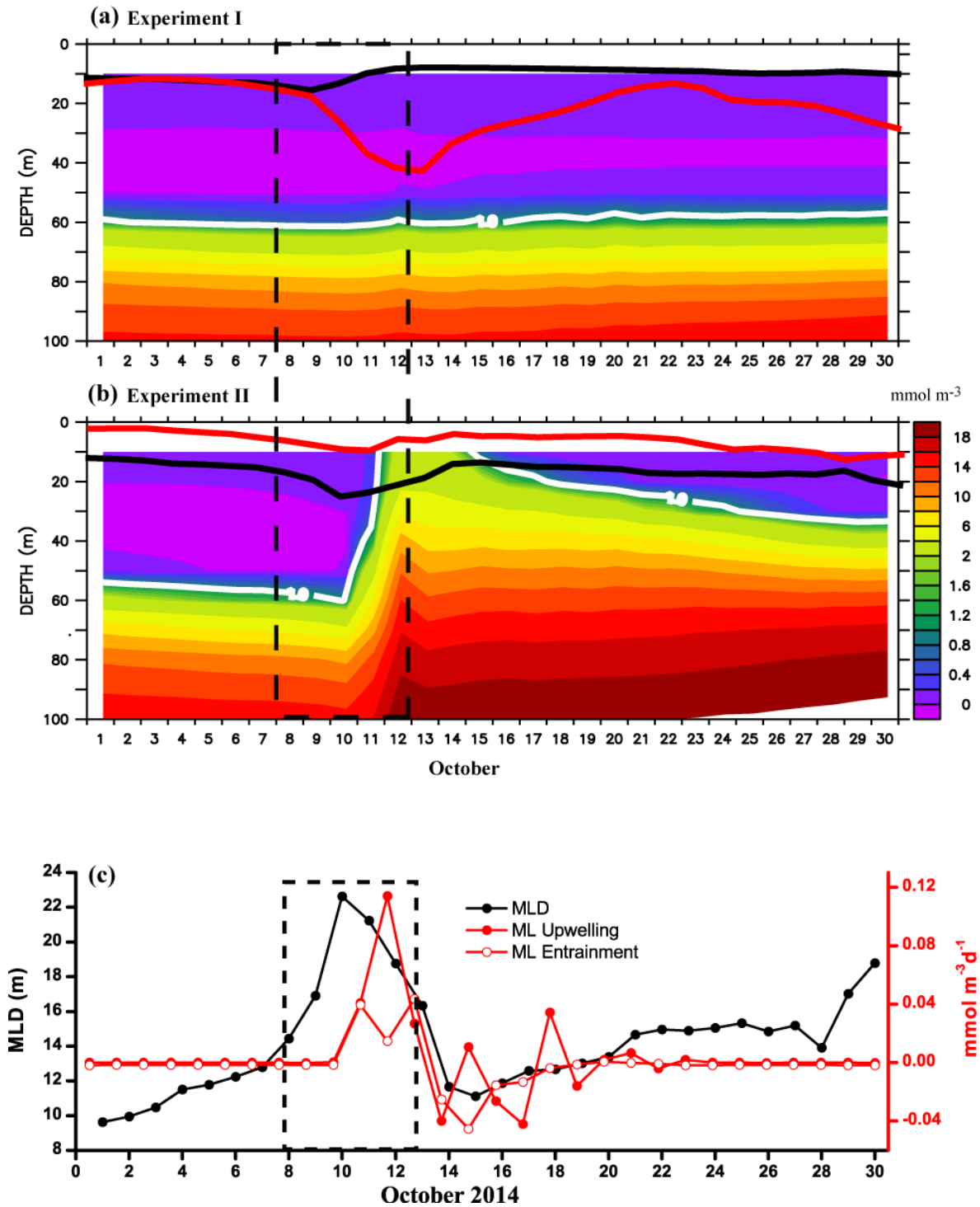


Figure 10. Time series of the vertical structure of water column nitrate [averaged over the region 84–86°E and 15–17°N] in (a) Experiment I and (b) Experiment II. (c) Time series of mixed layer depth (black line), upwelling term (red filled circle), and entrainment term (red circle) computed using mixed layer nitrate budget. In Figures 10a and b, white contours indicate the 1 mmol m^{-3} nitrate. Black contours indicate MLD, and red contours indicate BLT. The black dashed rectangle represents the cyclone period.

In Experiment I, the nitrate concentrations in the upper 50 m water column were less than 0.05 mmol m^{-3} ($\pm 0.02 \text{ mmol m}^{-3}$), indicating the oligotrophic region (Figure 10a). During all three

phases of the cyclone, nitrate concentrations were less than 0.05 mmol m^{-3} in Experiment I. While, in Experiment II, nitrate concentrations were much higher ($> 7 \text{ mmol m}^{-3}$) than the Experiment I (Figure 10b) during phase 2 in the upper 50 m. For example, at 50 m depth, the nitrate concentration was $< 0.05 \text{ mmol m}^{-3}$ in Experiment I, while it was $> 7 \text{ mmol m}^{-3}$ in Experiment II. In addition, we have compared the modelled nitrate from the World Ocean Atlas 2013 (WOA 2013) during October (Figure S9). The modelled nitrate distribution showed good comparison in the subsurface layers, however the upwelling starts in the modelled nitrate much before the period of cyclone, by the end of July (Figure S9b). This is mainly due to the very limited numbers of in situ nitrate profiles used in WOA13. Based on the above, we believe that comparison of modelled nitrate with WOA13 data in the euphotic zone may not be appropriate to compare for a specific year. As no other better data is available to compare with the model data, we have used WOA13 in the present study. But a good comparison of model-derived *Chla* with satellite and Argo data (Figure S7) indicate that the model reproduced surface and subsurface chlorophyll production during the cyclone passage. It is an indirect indication of the nitrate variability in the euphotic zone during the cyclone period.

In Experiment I, the MLD did not show much variability during phase 2 (Figure 10a; black line), and BLT increased from 15 m to 40 m (Figure 10a; red line). The deepening of the BLT in the absence of cyclone winds during Experiment I was mainly due to the increase in freshwater flux at the surface due to heavy rainfall during the cyclone (Figure 6c and 6g). Lack of strong cyclone winds in Experiment I could not initiate upwelling. While in Experiment II, during the cyclone period, initially, the BLT increased slightly, along with the deepening of the mixed layer (Figure 10b; black line). In the following days, when the cyclone intensified, the BLT and MLD decreased (Figure 10b; red line). We also computed the individual role of upwelling and entrainment of nitrate in the mixed layer during the cyclone period using the mixed layer budget analysis of nitrate (Resplandy et al., 2011) (Figure 10c). The upwelling term showed positive values on 11th and 12th October 2014 (Figure 10 c; filled red circle), while the entrainment term showed values close to zero (Figure 10 c; red circle). It further confirmed that the upwelling of nitrates induced by the cyclone winds was the dominant mechanism of *Chla* bloom after the cyclone passage. Consistent with the model, Argo data showed ~ 20 m MLD and ~ 12 m BLT before the cyclone (on 5th October 2014) (Figure S10). The MLD deepened from 20 m to 45 m, and the barrier layer disappeared during the cyclone (on 10th October 2014). The MLD again shoaled after 10 days of the cyclone and reached back 15 m, whereas BLT was at 5m (Figure S10). The difference in the MLD and absence of barrier layer on 10th October 2014 in figure S10 might be due to the absence of rainfall (freshwater flux) as Argo was located outside the eddy region.

In Experiment II, when the cyclone passed over the cyclonic eddy region, the strong wind speed (Figure S11; black line) led to an increase in wind stress, which resulted a divergent. We also calculated the Ekman pumping velocity (EPV), which reached a maximum value of $2.5 \times 10^{-5} \text{ m s}^{-1}$ on 11th October 2014 (Figure S11; red line). Though the MLD reached a maximum value of 22 m on 10th October 2014, from 11th onwards, MLD started shoaling and reached a minimum value of 11 m on 14th October 2014. On 15th October 2014, integrated Chla reached a maximum value of 140 mg m^{-2} (integrated Chla increased from 82.5 mg m^{-2} to 140 mg m^{-2}). It indicated that positive EPV resulted in the upwelling of cold nutrient-rich water to the mixed layer (Figure 10b), which subsequently led to shoaling of the mixed layer. The increased wind intensity (Figure S11; black line) led to a divergent of positive EPV (Figure S11; red line), which raised the isotherms approximately 50 m and resulted shoaling of the nitracline to the mixed layer (Figure 10b). Hence, the above analysis shows that during the cyclone, the mixed layer slightly deepens, and nutrient entrainment occurs. Though the rate of mixed layer deepening was very small, the vertical distribution of nitrate shows shoaling of nitracline due to strong upwelling induced by the cyclonic winds, which led to the upwelling of nutrients to the mixed layer and increased the Chla production (Figure 9b).

We further explored, in the absence of a pre-existing cyclonic eddy, what would be the intensity of the Chla bloom when the cyclone alone passed over the region. To understand that, we selected a small region (shown as a thick black box in Figure 1) along the cyclone track, where eddy was absent. Figure S12a indicates the vertical structure of Chla when eddy was absent, and Figure S12b indicates the Chla when both eddy and cyclone co-exist. Though Chla increased during the cyclone period (Figure S12a), its magnitude was much lesser. This confirms that during the post-monsoon season, the interaction of eddy-cyclone play a major role in the Chla production after the cyclone passage.

3.3 Discussion

In BoB, the strong stratification during the monsoon and post-monsoon seasons inhibits the nutrient transport from subsurface depth to the euphotic zone and makes the region strongly oligotrophic. In such oligotrophic region, only physical processes like mesoscale eddies (Prasanna Kumar et al., 2004) and tropical cyclones (Babin et al., 2004; Tummala et al., 2009; Vidya et al., 2017; Vinayachandran & Mathew, 2003) can pump nutrients from the subsurface water to the surface and increase the Chla concentration. In the present study, using an eddy-resolving coupled physical-biological model, we show that during the post-monsoon season, strong stratification in the northern BoB inhibits the eddy-driven upwelling of nutrients in the upper ocean. However, the

passage of cyclone Hudhud led to the intensification of the pre-existing cyclonic eddy, and the deepening of the MLD caused a phytoplankton bloom at a higher rate. Several studies (Chacko, 2017; Liu et al., 2009; Sun et al., 2014; Zheng et al., 2008, 2010) have shown that pre-existing cyclonic eddy provides an unbalanced thermodynamic structure (SST and water column stability), which helps to bring the cold nutrient-rich subsurface water to the surface and enhance the phytoplankton production. Using modeling study, Liu et al. (2009) showed that in the south China Sea, pre-existing cyclonic eddy strengthens the upper ocean upwelling and the significant increase of nutrient concentration which led to the development of phytoplankton bloom. Zheng et al. (2008) showed the pre-existing cyclonic eddy in the western North Pacific provides an unstable thermodynamic structure. Chacko (2017) showed that in the BoB, pre-existing cyclonic eddy lowers the translation speed of cyclone Hudhud and enhances the vertical pumping of nutrients to the euphotic zone, which resulted in elevated phytoplankton bloom.

Our study is in line with the study by Zheng et al. (2008), where their study showed that the pre-existing cyclonic eddy provides a favourable environment for the cyclone to the ready upwelling of cold nutrient-rich water to the upper ocean in the western North Pacific. But, here in the BoB, cyclonic eddy intensified after the passage of cyclone Hudhud, and the resultant eddy-cyclone interaction initiated the phytoplankton bloom. Sun et al. (2014) and Lu et al. (2016) showed that pre-existing cyclonic eddy conditions could increase the cooling time and phytoplankton bloom in the South China Sea (SCS). Zheng et al. (2008, 2010) showed that in the northwestern Pacific, pre-existing cyclonic eddy provides weak stratification, which results in the easy entrainment of cold nutrient-rich water to the surface. Though the strong stratification during the post-monsoon season inhibits the eddy-driven upwelling and subsequent SST cooling (Neetu et al., 2012), the present study showed that passage of cyclone Hudhud along the eddy region provided a favourable condition for the weakening of the stratification and upwelling of nutrients to the mixed layer.

When cyclone Hudhud (category 3) enters the cyclonic eddy region, the SST reached its minimum value. After the cyclone passage, the strong cyclone winds in the region reduced the BLT and thus accelerated SST cooling ($\sim 2.5^{\circ}\text{C}$). Though the intensity of cyclonic eddy increases, SST resumed its warming after four days of the cyclone passage. This indicates the inability of the cyclonic eddy to drive upwelling in the absence of a cyclone. The nitracline was always below the mixed layer when the cyclone was absent. However, the passage of cyclone Hudhud in the cyclonic eddy region led to the upwelling, which shoaled the mixed layer from 22 m to 11 m (~ 11 m) and favoured vertical supply of nitrate to the mixed layer subsequently triggered the *Chl a* bloom.

Anandh et al. (2020) and Patnaik et al. (2014) showed that during the passage of cyclone over the eddy, the cyclone's intensity increased in the BoB. Using observational data, Gordon et al. (2017) showed that rapid intensification and transformation of anticyclonic eddy occurred after the passage of a tropical cyclone in the BoB. All the above studies highlighted that eddy plays an important role in the intensification and dissipation of BoB cyclones. Though the prevailing winds were strong over the region, the strong stratification in the northern BoB inhibits the upwelling and thus led to the less entrainment of nutrient to the surface, which subsequently affected *Chla* production. Vidya et al. (2017) showed two times enhancement in the surface *Chla*/phytoplankton production after the cyclone passage. However, most of the time, eddy and cyclone co-occur in BoB. Hence, it was not possible to quantify the role of individual processes towards the *Chla*/phytoplankton production.

The strong cyclone winds during the cyclone Hudhud led to the upwelling of nutrients to the mixed layer and consequently led to the increased *Chla* concentration after three days of the cyclone. Without the cyclone winds, the nitrate in the upper 50 m water column was less than 0.5 mmol m^{-3} . This indicates that the strong winds during the cyclone help upwelling, reduce the BLT, thus by reducing the intensity of the stratification and allow upwelling of the nutrient-rich waters to the mixed layer. In the absence of cyclone winds, the strong water column stratification (as indicated by the deepened isotherms) does not allow the eddy-driven upwelling and thus restrict the *Chla* bloom. We show that cyclonic eddy can not initiate the eddy-driven upwelling and consequent upper ocean cooling during the post-monsoon season in the absence of strong cyclone winds.

The present study emphasizes that cyclone-eddy interaction during the post-monsoon season helps to break the strong stratification through wind-driven upwelling. The shoaling of the mixed layer led to the upwelling of nitrate from 0.5 mmol m^{-3} to 7 mmol m^{-3} and further enhanced phytoplankton production. We show that the cyclone-eddy interaction in the BoB led to 70 % increase in integrated *Chla* in the upper 100 m water column after the passage of Hudhud. Our results are consistent with the studies of Liu & Tang (2018) in the South China Sea. Using *in situ* observations and satellite measurements, Maneesha et al. (2012) showed strong upper ocean variability in the BoB associated with ocean-atmosphere interaction due to the cyclone. The present study also showed the ocean-atmosphere interaction due to cyclone Hudhud in the BoB.

3.4 Limitations of the study

In the present study, though the physical model had run for ten years, the biological model had run for only ten months. The long-time spin-up period in the biological model is required for the study to predict biogeochemical state variables. The present study differs by far from the perspective

of performance evaluation of a biogeochemical model. Rather, we utilized a simple set of numerical experiments confined to recommendations based on the detailed literature survey to investigate the potential significance of cyclone winds to induce upwelling of biogeochemical properties. The increase in model spin-up could certainly improve the accuracy of *Chla* fields. Still, the observed spatiotemporal properties are not expected to undergo contrasting changes considering the governing physical processes.

4. Conclusion

In this study, the interaction of the pre-existing cyclonic eddy and cyclone (Hudhud) was studied using ROMS coupled with an established NPZD model. In the BoB, during the post-monsoon season, strong stratification along with a thick barrier layer inhibited eddy-driven upwelling of nutrients to the mixed layer and restricted the phytoplankton production. However, the presence of cyclone in the cyclonic eddy region played a critical role in the development of phytoplankton bloom by reducing the water column stability and increasing the intensity of wind-driven upwelling. The above mechanism helped to break the strong stratification, which increased the nitrate from 0.5 mmol m^{-3} to 7 mmol m^{-3} and further enhanced phytoplankton production. The present study showed that during the post-monsoon season, cyclonic eddy unaccompanied with cyclone Hudhud could not induce the phytoplankton bloom. This eddy-cyclone interaction strengthened bottom-up processes in which nutrients entrain to the mixed layer, which led to the development of phytoplankton bloom. Our model showed how the nitrate and corresponding *Chla* concentration increased when the cyclone Hudhud crossed over the pre-existing cyclonic eddy region. This study using a numerical model showed that atmosphere-ocean coupled processes play an important role in phytoplankton growth in the BoB. Note that the present model solutions corresponding to biogeochemical fields could have improved representation with a more extended spin-up period with ROMS bio-fennel model (preferably 1-2 years). Furthermore, the authors suggest multiple cyclone case studies using a coupled atmosphere-ocean-bio model to have a deeper insight into complex interactions of cyclone induced biogeochemical response of the upper ocean.

Acknowledgements:

Authors thank the Director, CSIR-National Institute of Oceanography (NIO), Goa and Director, National Center for Polar and Ocean Research (NCPOR), Goa, for all support and encouragement. Model simulations were carried out in HPC Pravah at CSIR-NIO, Goa. We sincerely thank Associate Editor Roxy Mathew Koll and the two anonymous reviewers for their valuable comments and suggestions, which significantly improved the quality of the manuscript. PJV acknowledges DST-

SERB for the fast track young scientist fellowship. Details of the data sets used for this study are mentioned in the data and method section. The NCPOR contribution number is xxxx. The NIO contribution number is XXXX.

Reference:

- Anandh, T.S., Das, B.K., Kuttippurath, J., Chakraborty, A., 2020. A coupled model analyses on the interaction between oceanic eddies and tropical cyclones over the Bay of Bengal. *Ocean Dyn.* <https://doi.org/10.1007/s10236-019-01330-x>
- Babin, S. M., Carton, J. A., Dickey, T. D., & Wiggert, J. D. (2004). Satellite evidence of hurricane-induced phytoplankton blooms in an oceanic desert. *Journal of Geophysical Research C: Oceans*.
- Barnston, A.G., Tippett, M.K. Predictions of Nino3.4 SST in CFSv1 and CFSv2: a diagnostic comparison. *Clim Dyn* 41, 1615–1633 (2013). <https://doi.org/10.1007/s00382-013-1845-2>
- Chacko, N. (2017). Chlorophyll bloom in response to tropical Cyclone Hudhud in the Bay of Bengal: Bio-Argo subsurface observations. *Deep-Sea Research Part I: Oceanographic Research Papers*. <https://doi.org/10.1016/j.dsr.2017.04.010>
- Chen, G., Wang, D., & Hou, Y. (2012). The features and interannual variability mechanism of mesoscale eddies in the Bay of Bengal. *Continental Shelf Research*. <https://doi.org/10.1016/j.csr.2012.07.011>
- Chen, Xiaoyan, Pan, D., Bai, Y., He, X., Chen, C. T. A., & Hao, Z. (2013). Episodic phytoplankton bloom events in the Bay of Bengal triggered by multiple forcings. *Deep-Sea Research Part I: Oceanographic Research Papers*. <https://doi.org/10.1016/j.dsr.2012.11.011>
- Chen, Xinping, Liu, C., O’Driscoll, K., Mayer, B., Su, J., & Pohlmann, T. (2013). On the nudging terms at open boundaries in regional ocean models. *Ocean Modelling*. <https://doi.org/10.1016/j.ocemod.2013.02.006>
- Dong, S., S. L. Garzoli, and M. Baringer (2009), An assessment of the seasonal mixed layer salinity budget in the Southern Ocean, *J. Geophys. Res.*, 114, C12001, doi:10.1029/2008JC005258
- Eppley, R. W., & Renger, E. H. (1988). Nanomolar increase in surface layer nitrate concentration following a small wind event. *Deep Sea Research Part A, Oceanographic Research Papers*. [https://doi.org/10.1016/0198-0149\(88\)90004-0](https://doi.org/10.1016/0198-0149(88)90004-0)
- Fennel, K., Hetland, R., Feng, Y., & Dimarco, S. (2011). A coupled physical-biological model of the Northern Gulf of Mexico shelf: Model description, validation and analysis of phytoplankton variability. *Biogeosciences*. <https://doi.org/10.5194/bg-8-1881-2011>
- Fennel, Katja, Wilkin, J., Levin, J., Moisan, J., O’Reilly, J., & Haidvogel, D. (2006). Nitrogen cycling in the Middle Atlantic Bight: Results from a three-dimensional model and implications for the North Atlantic nitrogen budget. *Global Biogeochemical Cycles*, 20(3), 1–14.

<https://doi.org/10.1029/2005GB002456>

- Fennel, Katja, Wilkin, J., Previdi, M., & Najjar, R. (2008). Denitrification effects on air-sea CO₂ flux in the coastal ocean: Simulations for the northwest North Atlantic. *Geophysical Research Letters*, 35(24), 1–5. <https://doi.org/10.1029/2008GL036147>
- Flather, R. A. (1975). A tidal model of the north-west European continental shelf. *MEM. SOC. ROYALE SCI. DE LIEGE, SER.6*.
- Gordon, A.L., Shroyer, E., Murty, V.S.N., 2017. An Intrathermocline Eddy and a tropical cyclone in the Bay of Bengal. *Sci. Rep.* <https://doi.org/10.1038/srep46218>
- Goswami, B. B., M. Deshpande, P. Mukhopadhyay, S. K. Saha, S. A. Rao, R. Murthugudde, and B. N. Goswami (2014), Simulation of monsoon intraseasonal variability in NCEP CFSv2 and its role on systematic bias, *Clim. Dyn.*, 43(9-10), 2725– 2745, doi:10.1007/s00382-014-2089-5
- Kara, A. B., Rochford, P. A., & Hurlburt, H. E. (2000). An optimal definition for ocean mixed layer depth. *Journal of Geophysical Research: Oceans*. <https://doi.org/10.1029/2000jc900072>
- Kim, H., Webster, P.J. & Curry, J.A. Seasonal prediction skill of ECMWF System 4 and NCEP CFSv2 retrospective forecast for the Northern Hemisphere Winter. *Clim Dyn* 39, 2957–2973 (2012). <https://doi.org/10.1007/s00382-012-1364-6>
- Liu, F., & Tang, S. (2018). Influence of the Interaction Between Typhoons and Oceanic Mesoscale Eddies on Phytoplankton Blooms. *Journal of Geophysical Research: Oceans*. <https://doi.org/10.1029/2017JC013225>
- Liu, X., Wang, M., & Shi, W. (2009). A study of a Hurricane Katrina–induced phytoplankton bloom using satellite observations and model simulations. *Journal of Geophysical Research*, 114(C3), C03023. <https://doi.org/10.1029/2008JC004934>
- Locarnini, R. A., Mishonov, A. V., Antonov, J. I., Boyer, T. P., Garcia, H. E., Baranova, O. K., ... Seidov, D. (2013). *World Ocean Atlas 2013. Vol. 1: Temperature*. S. Levitus, Ed.; A. Mishonov, Technical Ed.; NOAA Atlas NESDIS. <https://doi.org/10.1182/blood-2011-06-357442>
- Lu, Z., Wang, G., & Shang, X. (2016). Response of a pre-existing cyclonic ocean eddy to a typhoon. *Journal of Physical Oceanography*. <https://doi.org/10.1175/JPO-D-16-0040.1>
- Maneesha, K., Sarma, V. V. S. S., Reddy, N. P. C., Sadhuram, Y., Ramana Murty, T. V., Sarma, V. V., & Dileep Kumar, M. (2011). Meso-scale atmospheric events promote phytoplankton blooms in the coastal Bay of Bengal. *Journal of Earth System Science*. <https://doi.org/10.1007/s12040-011-0089-y>
- Maneesha, K., Murty, V. S. N., Ravichandran, M., Lee, T., Yu, W., & McPhaden, M. J. (2012). Upper ocean variability in the Bay of Bengal during the tropical cyclones Nargis and Laila. *Progress in Oceanography*. <https://doi.org/10.1016/j.pocean.2012.06.006>
- Marchesiello, P., McWilliams, J. C., & Shchepetkin, A. (2001). Open boundary conditions for long-term integration of regional oceanic models. *Ocean Modelling*. [https://doi.org/10.1016/S1463-5003\(00\)00013-5](https://doi.org/10.1016/S1463-5003(00)00013-5)

- Morel A, Berthon JF (1989) Surface pigments, algal biomass profiles and potential production of the euphotic layer: relationships reinvestigated in view of remote-sensing applications. *Limnol Oceanogr* 34:1545–1562
- Neetu, S., Lengaigne, M., Vincent, E. M., Vialard, J., Madec, G., Samson, G., ... Durand, F. (2012). Influence of upper-ocean stratification on tropical cyclone-induced surface cooling in the Bay of Bengal. *Journal of Geophysical Research: Oceans*. <https://doi.org/10.1029/2012JC008433>
- Vidya P.J., Das, S., & Murali.R, M. (2017). Contrasting Chl-a responses to the tropical cyclones Thane and Phailin in the Bay of Bengal. *Journal of Marine Systems*. <https://doi.org/10.1016/j.jmarsys.2016.10.001>
- Patnaik, K. V. K. R. K., Maneesha, K., Sadhram, Y., Prasad, K. V. S. R., Ramana Murty, T. V., & Brahmananda Rao, V. (2014). East India Coastal Current induced eddies and their interaction with tropical storms over Bay of Bengal. *Journal of Operational Oceanography*. <https://doi.org/10.1080/1755876X.2014.11020153>
- Patra, P. K., Kumar, M. D., Mahowald, N., & Sarma, V. V. S. S. (2007). Atmospheric deposition and surface stratification as controls of contrasting chlorophyll abundance in the North Indian Ocean. *Journal of Geophysical Research: Oceans*. <https://doi.org/10.1029/2006JC003885>
- Pokhrel, S., Rahaman, H., Parekh, A. et al. Evaporation-precipitation variability over Indian Ocean and its assessment in NCEP Climate Forecast System (CFSv2). *Clim Dyn* 39, 2585–2608 (2012). <https://doi.org/10.1007/s00382-012-1542-6>
- Prasanna Kumar, S., Muraleedharan, P. M., Prasad, T. G., Gauns, M., Ramaiah, N., de Souza, S. N., ... Madhupratap, M. (2002). Why is the Bay of Bengal less productive during summer monsoon compared to the Arabian Sea? *Geophysical Research Letters*. <https://doi.org/10.1029/2002gl016013>
- Prasanna Kumar, S., Nuncio, M., Narvekar, J., Kumar, A., Sardesai, S., De Souza, S. N., ... Madhupratap, M. (2004). Are eddies nature's trigger to enhance biological productivity in the Bay of Bengal? *Geophysical Research Letters*. <https://doi.org/10.1029/2003GL019274>
- Prasanna Kumar, S., Nuncio, M., Ramaiah, N., Sardesai, S., Narvekar, J., Fernandes, V., & Paul, J. T. (2007). Eddy-mediated biological productivity in the Bay of Bengal during fall and spring intermonsoons. *Deep-Sea Research Part I: Oceanographic Research Papers*. <https://doi.org/10.1016/j.dsr.2007.06.002>
- Price, J. F. (1981). Upper ocean response to a hurricane. *J. PHYS. OCEANOGR.*, 11,153-175.
- Rao, R. R., & Sivakumar, R. (2003). Seasonal variability of sea surface salinity and salt budget of the mixed layer of the north Indian Ocean. *Journal of Geophysical Research C: Oceans*. <https://doi.org/10.1029/2001jc000907>
- Resplandy, L., M. Lévy, G. Madec, S. Pous, O. Aumont, and D. Kumar (2011), Contribution of mesoscale processes to nutrient budgets in the Arabian Sea, *J. Geophys. Res.*, 116, C11007, doi:10.1029/2011JC007006.
- Sadhram, Y., Maneesha, K., & Murty, T. V. R. (2012). Intensification of Aila (May 2009) due to a warm core eddy in the north Bay of Bengal. *Natural Hazards*. <https://doi.org/10.1007/s11069-011-9837->

- Saha, S., Moorthi, S., Wu, X., Wang, J., Nadiga, S., Tripp, P., ... Becker, E. (2014). The NCEP climate forecast system version 2. *Journal of Climate*. <https://doi.org/10.1175/JCLI-D-12-00823.1>
- Sathyendranath, S.; Grant, M.; Brewin, R.J.W.; Brockmann, C.; Brotas, V.; Chuprin, A.; Doerffer, R.; Dowell, M.; Farman, A.; Groom, S.; Jackson, T.; Krasemann, H.; Lavender, S.; Martinez Vicente, V.; Mazeran, C.; Mélin, F.; Moore, T.S.; Müller, D.; Platt, T.; Regner, P.; Roy, S.; Steinmetz, F.; Swinton, J.; Valente, A.; Zühlke, M.; Antoine, D.; Arnone, R.; Balch, W.M.; Barker, K.; Barlow, R.; Bélanger, S.; Berthon, J.-F.; Beşiktepe, Ş.; Brando, V.E.; Canuti, E.; Chavez, F.; Claustre, H.; Crout, R.; Feldman, G.; Franz, B.; Frouin, R.; García-Soto, C.; Gibb, S.W.; Gould, R.; Hooker, S.; Kahru, M.; Klein, H.; Kratzer, S.; Loisel, H.; McKee, D.; Mitchell, B.G.; Moisan, T.; Muller-Karger, F.; O'Dowd, L.; Ondrusek, M.; Poulton, A.J.; Repecaud, M.; Smyth, T.; Sosik, H.M.; Taberner, M.; Twardowski, M.; Voss, K.; Werdell, J.; Wernand, M.; Zibordi, G. (2018): ESA Ocean Colour Climate Change Initiative (Ocean_Colour_cci): Version 3.1 Data. Centre for Environmental Data Analysis, 04 July 2018. doi:10.5285/9c334fbe6d424a708cf3c4cf0c6a53f5 <http://dx.doi.org/10.5285/9c334fbe6d424a708cf3c4cf0c6a53f5>
- Schott, F. A., & McCreary, J. P. (2001). The monsoon circulation of the Indian Ocean. *Progress in Oceanography*. [https://doi.org/10.1016/S0079-6611\(01\)00083-0](https://doi.org/10.1016/S0079-6611(01)00083-0)
- Shchepetkin, A. F., & McWilliams, J. C. (2005). The regional oceanic modeling system (ROMS): A split-explicit, free-surface, topography-following-coordinate oceanic model. *Ocean Modelling*, 9(4), 347–404. <https://doi.org/10.1016/j.ocemod.2004.08.002>
- Da Silva, R., Mazumdar, A., Mapder, T., Peketi, A., Joshi, R. K., Shaji, A., ... Molletti, S. K. (2017). Salinity stratification controlled productivity variation over 300 ky in the Bay of Bengal. *Scientific Reports*. <https://doi.org/10.1038/s41598-017-14781-3>
- Sun, L., Li, Y. X., Yang, Y. J., Wu, Q., Chen, X. T., Li, Q. Y., ... Xian, T. (2014). Effects of super typhoons on cyclonic ocean eddies in the western North Pacific: A satellite data-based evaluation between 2000 and 2008. *Journal of Geophysical Research C: Oceans*, 119(9), 5585–5598. <https://doi.org/10.1002/2013JC009575>
- Tummala, S.K., Mupparthy, R.S., Masuluri, N.K. and Nayak, S.R., 2009. Phytoplankton bloom due to Cyclone Sidr in the central Bay of Bengal. *Journal of Applied Remote Sensing*, 3(1), p.033547.
- Umlauf, L., & Burchard, H. (2003). A generic length-scale equation for geophysical turbulence models. *Journal of Marine Research*. <https://doi.org/10.1357/002224003322005087>
- Vidya, P. J., & Kumar, S. P. (2013). Role of mesoscale eddies on the variability of biogenic flux in the northern and central Bay of Bengal. *Journal of Geophysical Research: Oceans*, 118(10), 5760–5771. <https://doi.org/10.1002/jgrc.20423>
- Vinayachandran, P. N., & Mathew, S. (2003). Phytoplankton bloom in the Bay of Bengal during the northeast monsoon and its intensification by cyclones. *Geophysical Research Letters*. <https://doi.org/10.1029/2002GL016717>

- Warner, J. C., Sherwood, C. R., Arango, H. G., & Signell, R. P. (2005). Performance of four turbulence closure models implemented using a generic length scale method. *Ocean Modelling*. <https://doi.org/10.1016/j.ocemod.2003.12.003>
- Yuan, X., Wood, E. F., Luo, L., & Pan, M. (2011). A first look at Climate Forecast System version 2 (CFSv2) for hydrological seasonal prediction. *Geophysical Research Letters*, 38, L13402. <https://doi.org/10.1029/2011GL047792>
- Zheng, Z. W., Ho, C. R., Zheng, Q., Lo, Y. T., Kuo, N. J., & Gopalakrishnan, G. (2010). Effects of pre-existing cyclonic eddies on upper ocean responses to Category 5 typhoons in the western North Pacific. *Journal of Geophysical Research: Oceans*. <https://doi.org/10.1029/2009JC005562>
- Zheng, Z. W., Ho, C. R., & Kuo, N. J. (2008). Importance of pre-existing oceanic conditions to upper ocean response induced by Super Typhoon Hai-Tang. *Geophysical Research Letters*, 35(20), 1–5. <https://doi.org/10.1029/2008GL035524>
- Zhou Chaojie, Ding Xiaohua, Zhang Jie, Yang Jungang, Ma Qiang. 2018. An evaluation of sea surface height assimilation using along-track and gridded products based on the Regional Ocean Modeling System (ROMS) and the four-dimensional variational data assimilation. *Acta Oceanologica Sinica*, 37(9): 50–58, doi: 10.1007/s13131-018-1225-1
- Zuo, Z., Yang, S., Hu, Z. et al. Predictable patterns and predictive skills of monsoon precipitation in Northern Hemisphere summer in NCEP CFSv2 reforecasts. *Clim Dyn* 40, 3071–3088 (2013). <https://doi.org/10.1007/s00382-013-1772-2>
- Zweng, M. M., Reagan, J. R., Antonov, J. I., Locarnini, R. A., Mishonov, A. V., Boyer, T. P., ... Bidlle, M. M. (2013). *World Ocean Atlas 2013 Volume 2: Salinity*. S. Levitus, Ed.; A. Mishonov, Technical Ed.; NOAA Atlas NESDIS 74, 39 pp. NOAA Atlas NESDIS 74. <https://doi.org/10.1182/blood-2011-06-357442>

Supplementary material

Table S1: Overview of ROMS model configuration

Model	ROMS (3.7)
Dynamics	Hydrostatic
Map projection	Mercator
Model domain	SW: 5N & 75E NE: 30N & 100E
Model time step	Baroclinic – 60 s Barotropic – 30 time steps
Surface stretching parameters θ_s	7
Bottom stretching parameters θ_b	0.4
Vertical S-coordinate parameter (HC)	10 m
Vertical levels (σ)	40
Lateral boundary condition	Free surface – Chapman 2D UV – Flather 3D UV, T & S – Radiation + Nudging
Sponge	1500 km
Harmonic horizontal diffusion co-efficient for tracers	$10 \text{ m}^2 \text{ s}^{-1}$
Harmonic horizontal viscosity co-efficient for tracers	$100 \text{ m}^2 \text{ s}^{-1}$

Supplementary material

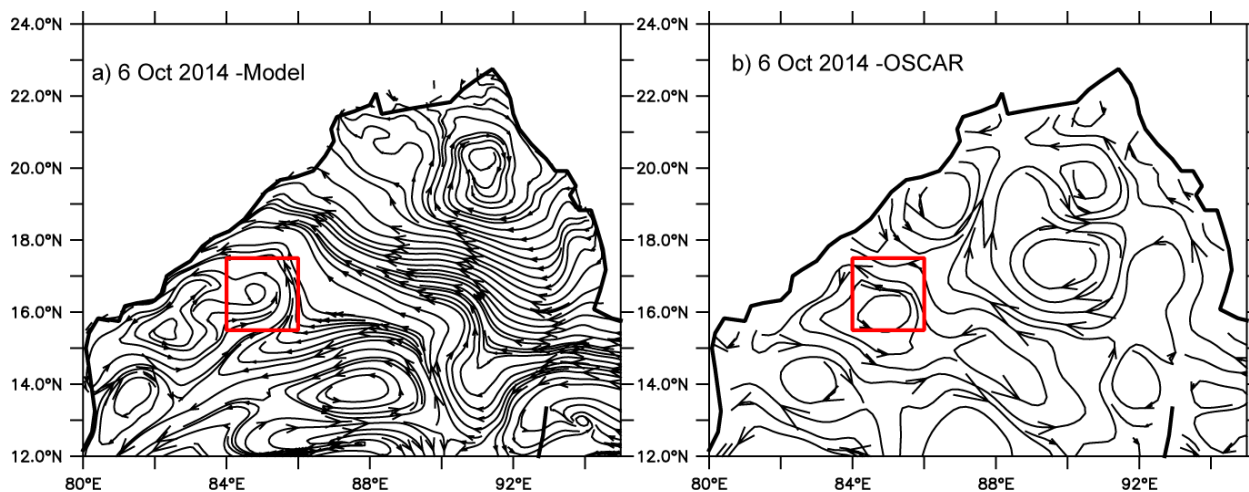


Figure S1. Spatial maps of surface currents from (a) model and (b) OSCAR data on 6th October 2014. The red rectangle indicates the study region.

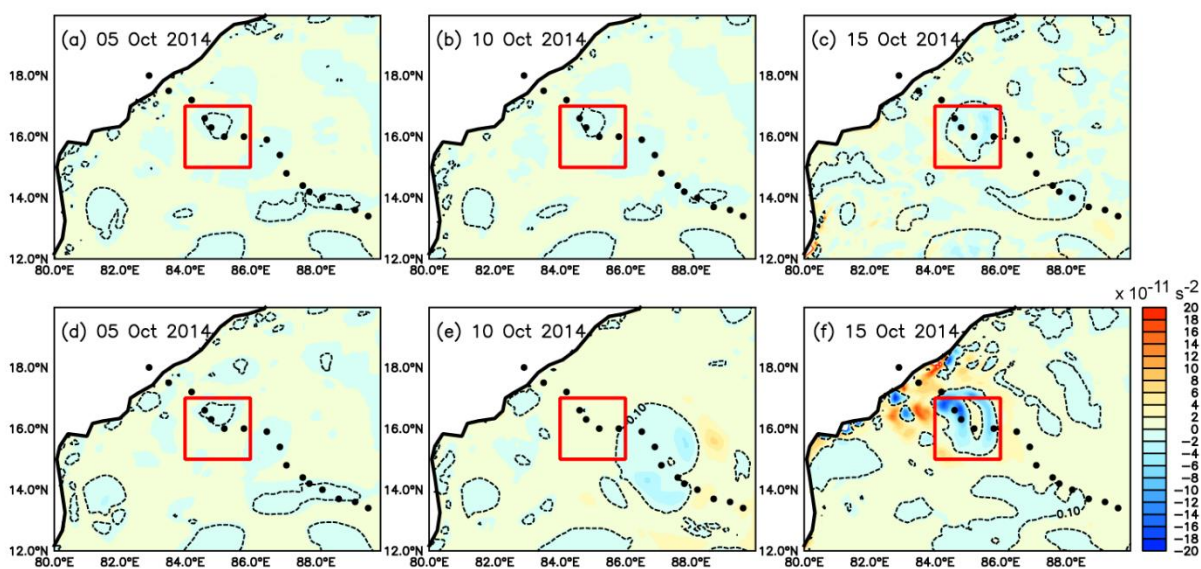
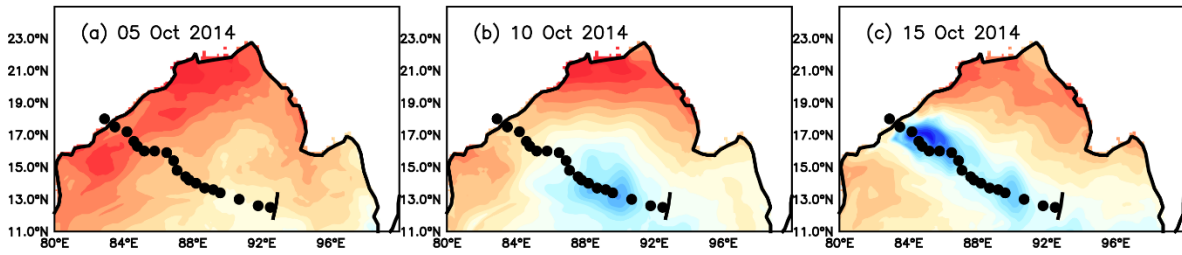


Figure S2: Okubo-Weiss parameter computed from the model currents in the upper 100m water column during Experiment 1 (a-c) and II (d-f). The red rectangle represents the region where cyclone and eddy co-exist.

Sea surface temperature from the model



Sea surface temperature from the satellite

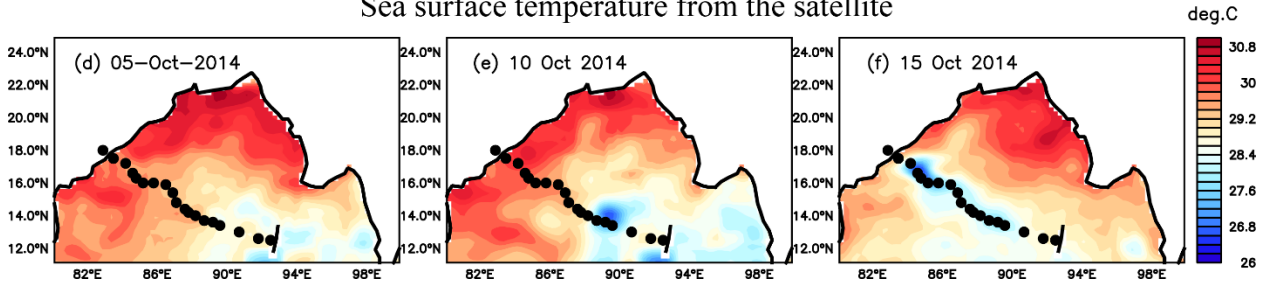


Figure S3. Comparison of SST from the model (a-c) versus satellite (d-f).

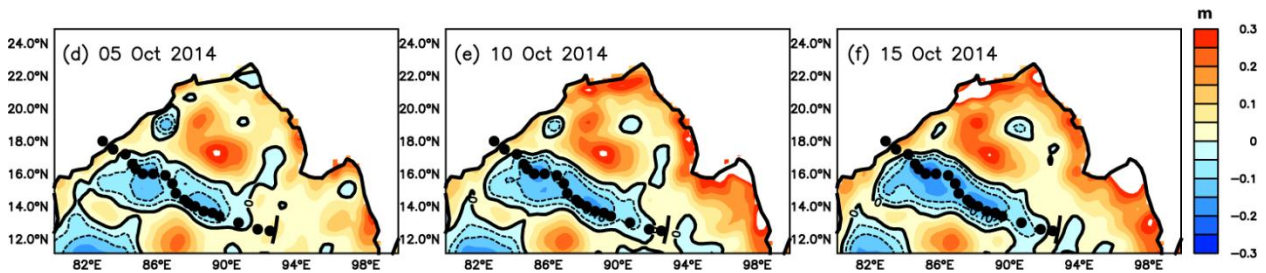
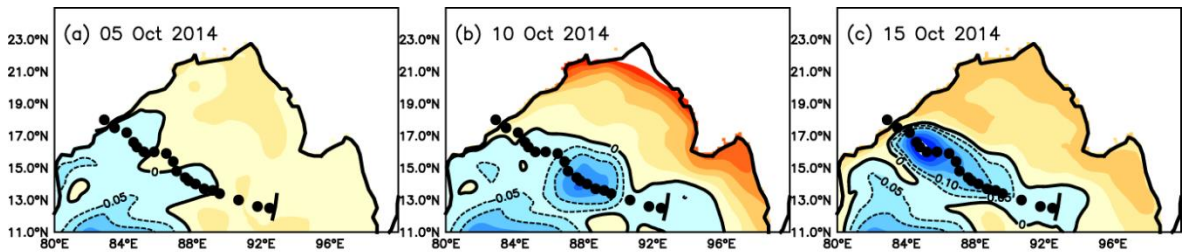


Figure S4. Comparison of SLA from the model (a-c) versus satellite (d-f).

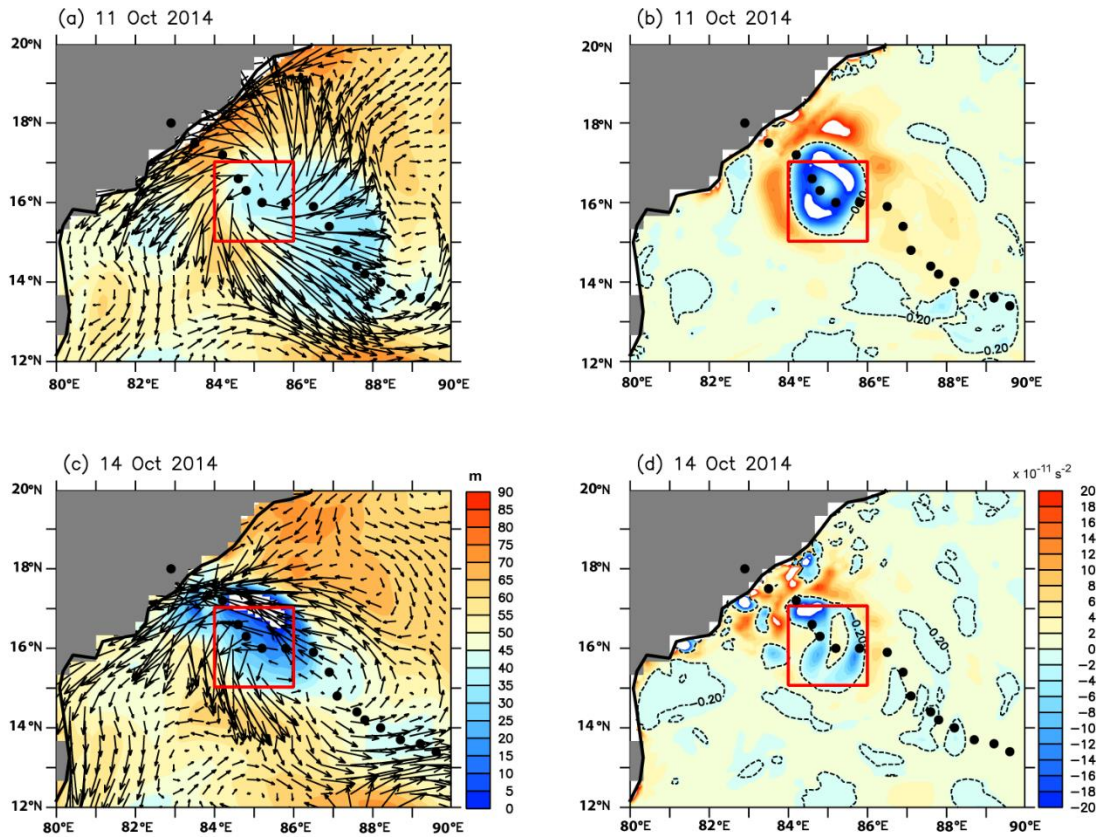


Figure S5. The spatial pattern of the depth of 26-degree isotherm overlaid with the currents in the upper 100 m from the model (a) 11th October 2014 and (c) 14th October 2014. Okubo-Weiss parameter computed from the model currents in the upper 100 m (b) 11th October 2014 and (d) 14th October 2014. The red rectangle represents the region where cyclone and eddy co-exist.

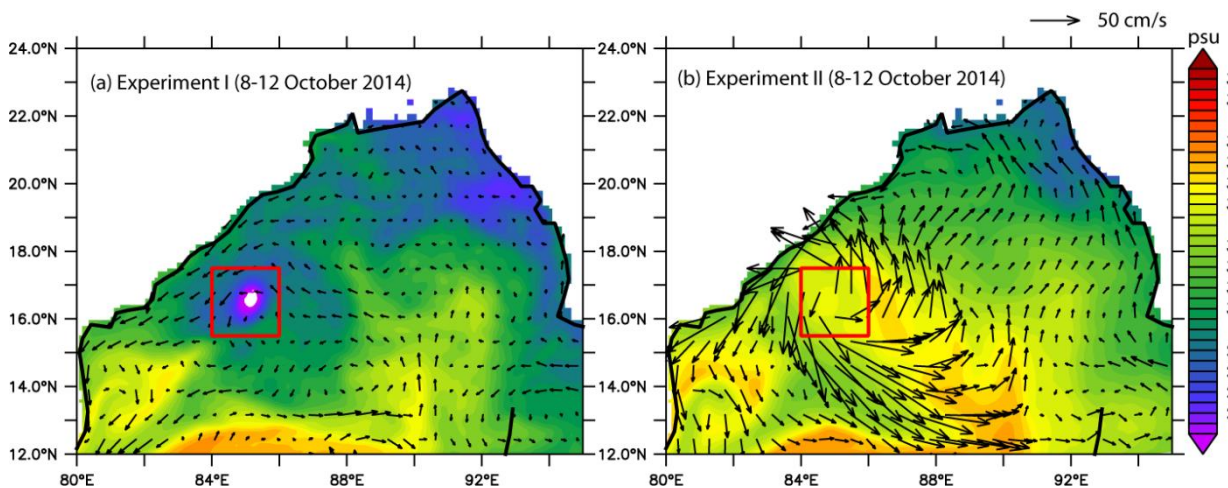


Figure S6. The spatial pattern of surface salinity overlaid with the currents during the cyclone period (averaged over the period 8-12th October 2014) from (a) Experiment I and (b) Experiment II. The red rectangle represents the region where cyclone and eddy co-exist.

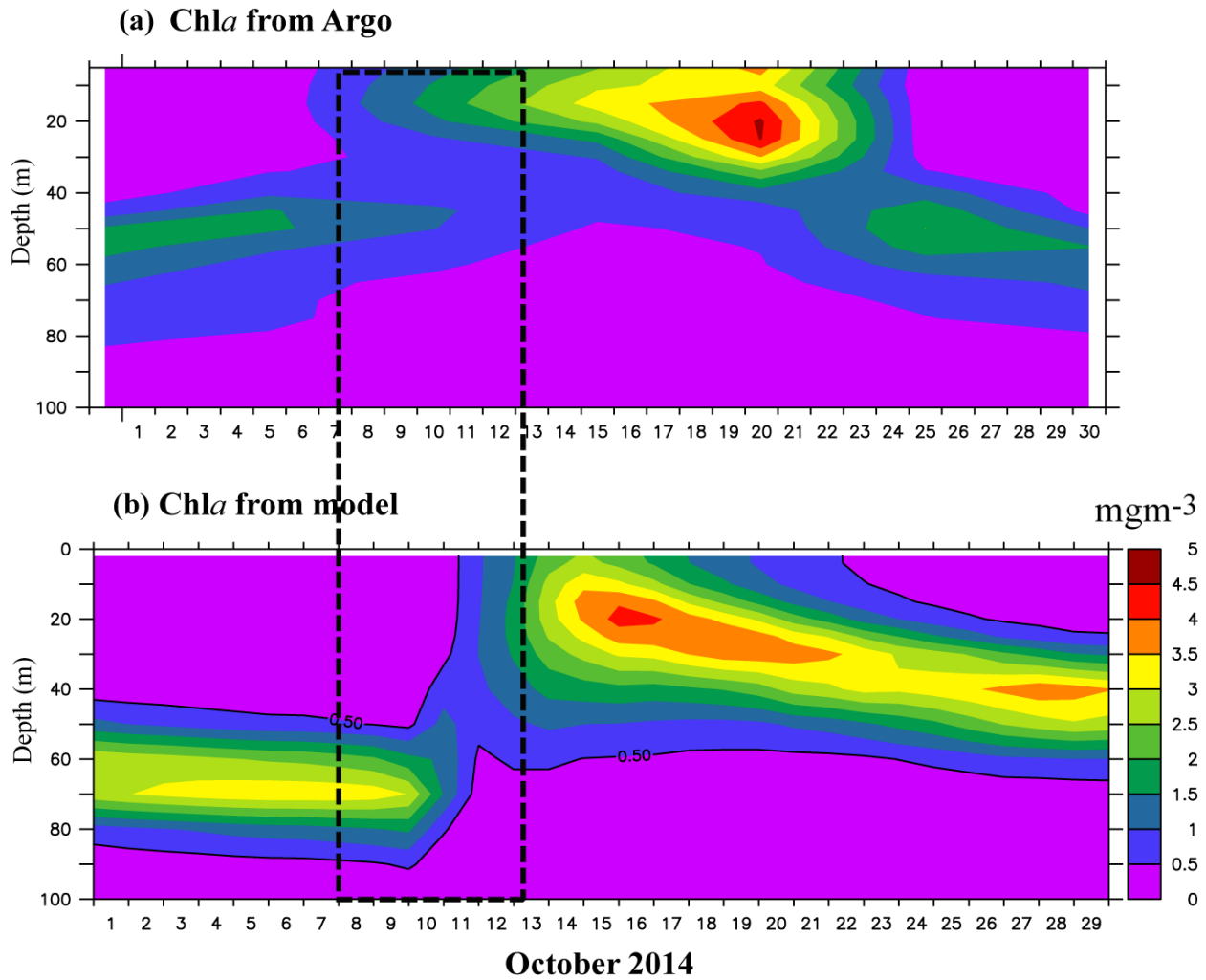


Figure S7: Comparison of the vertical structure of Chla from Argo and model. The modelled Chla is averaged over the region 84-86°E and 15-17°N. The black dashed rectangle represents the cyclone period.

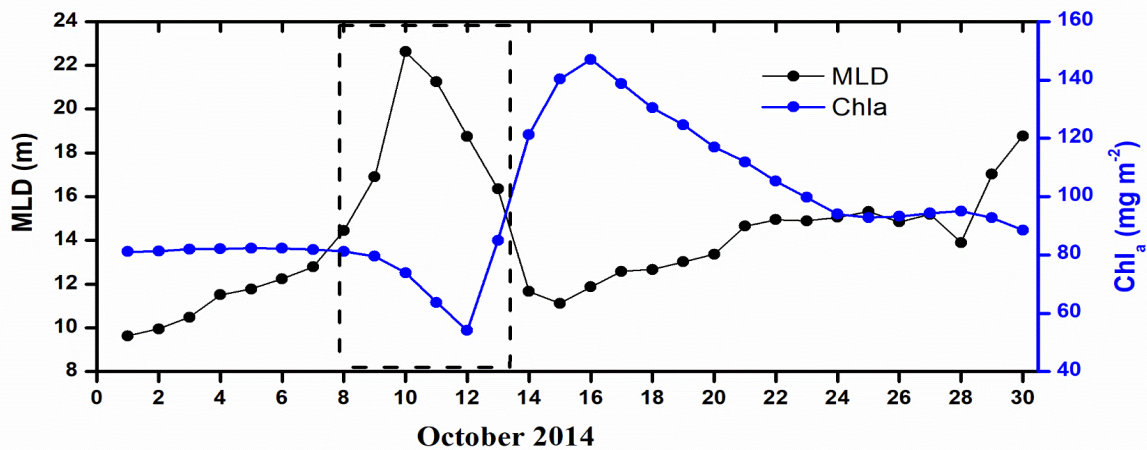


Figure S8. Time series of mixed layer depth (MLD; black line), Ekman pumping velocity (EPV; red line), and integrated Chla values in the upper 100 m (blue line) in the region 84-86°E and 15-17°N. The black dashed rectangle represents the cyclone period.

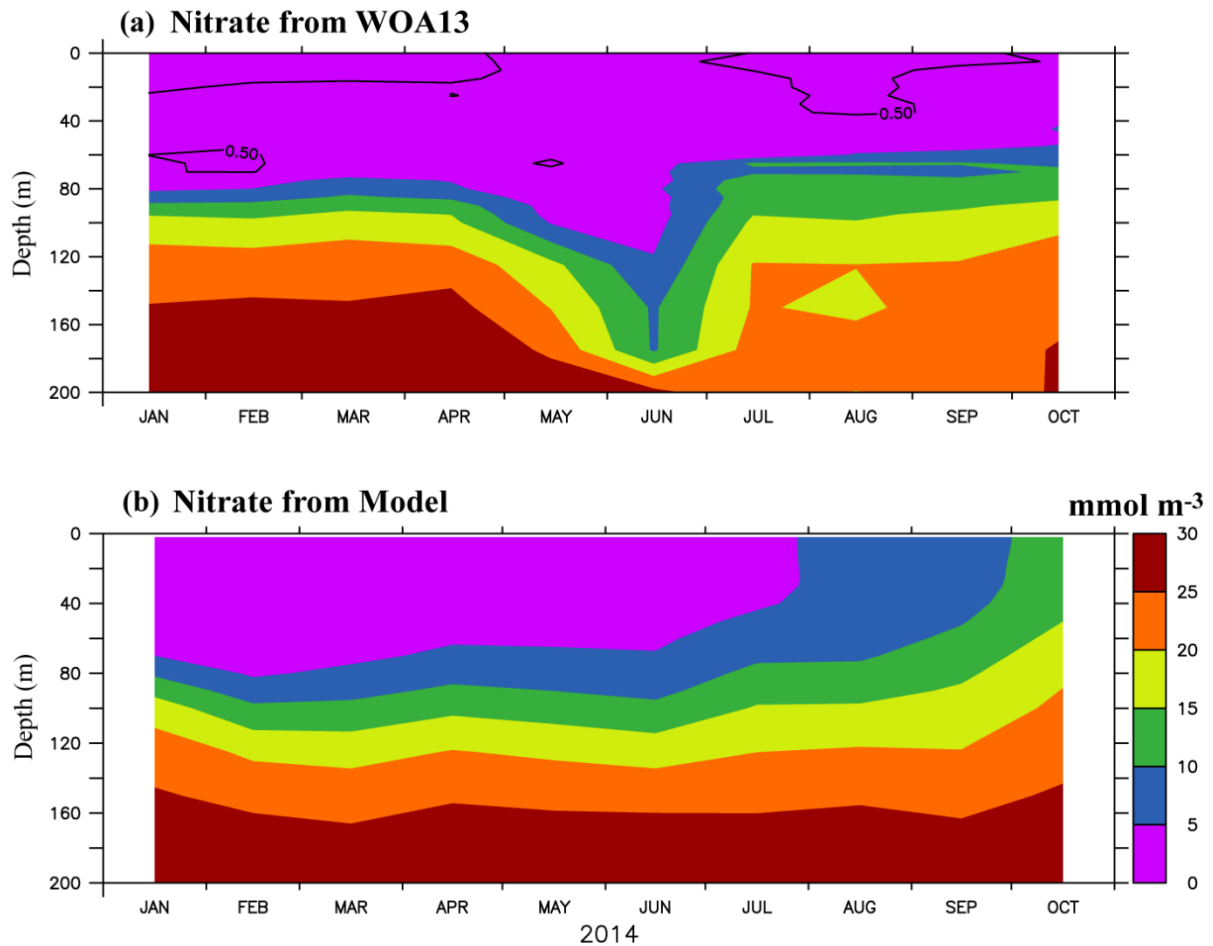


Figure S9. Time series of Nitrate from the (a) from WOA13 during January to October and (b) Model during 01 January – 31 October 2014 averaged over the region 84-86°E and 15-17°N.

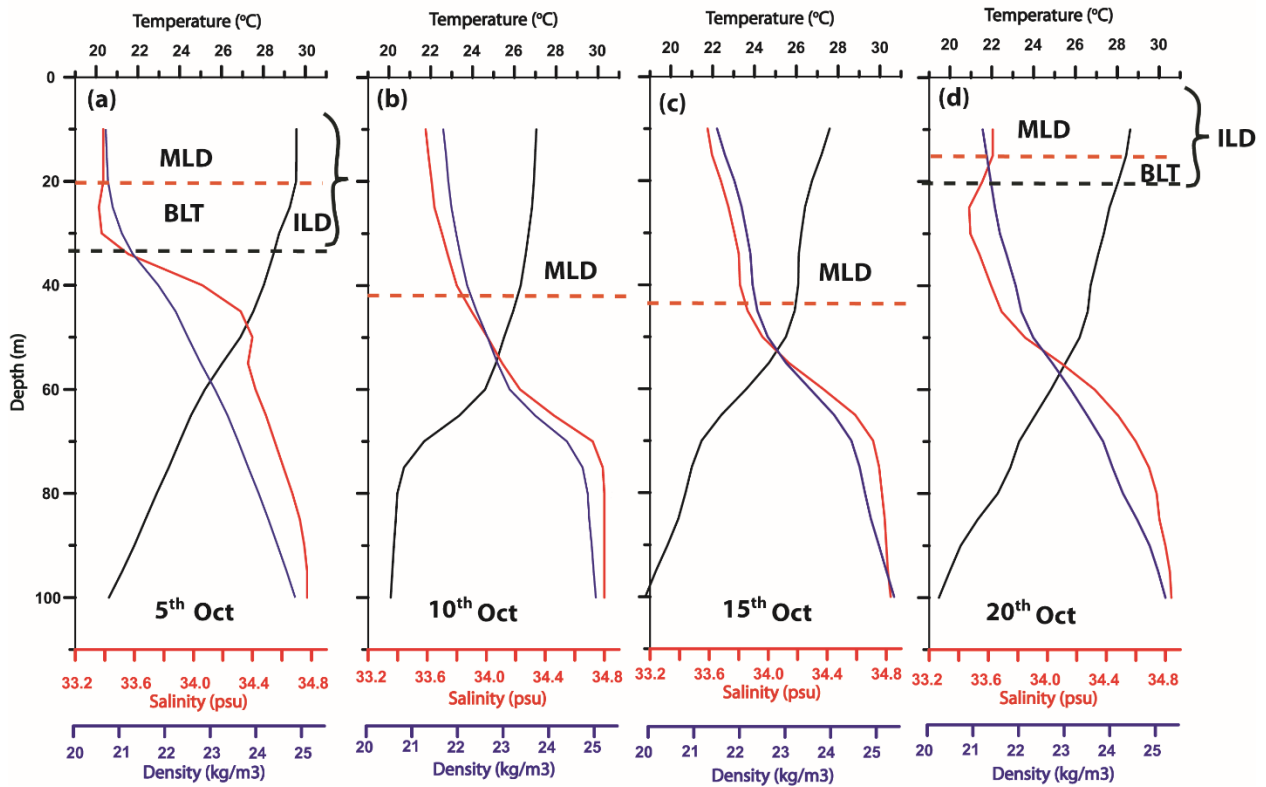


Figure S10. Mixed layer depth (MLD), Barrier layer thickness (BLT) computed from the Argo profile, which located along the cyclone track.

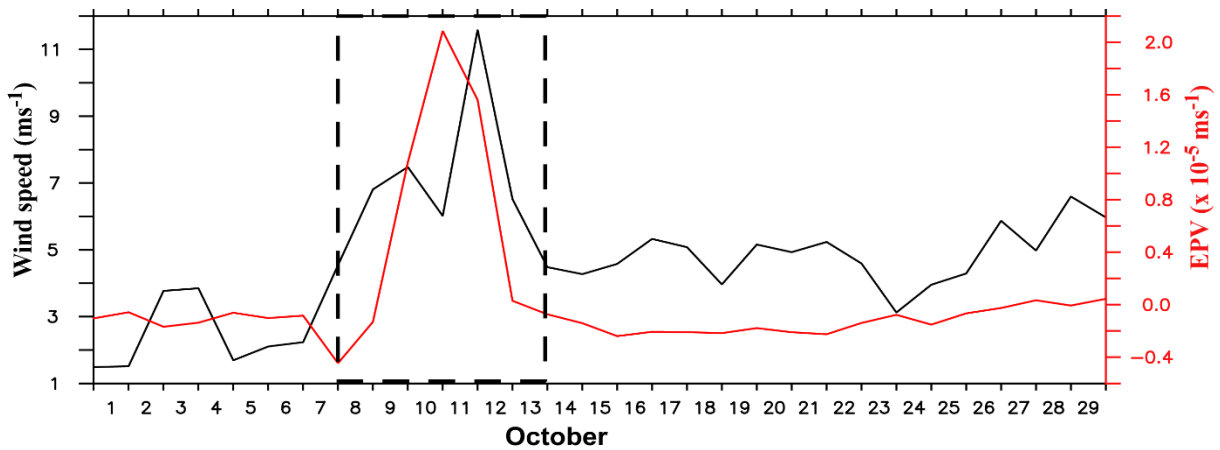


Figure S11: Wind speed (black line) and Ekman pumping velocity (EPV; red line) [averaged over the region 84-86°E and 15-17°N]. The black dashed rectangle represents the cyclone period.

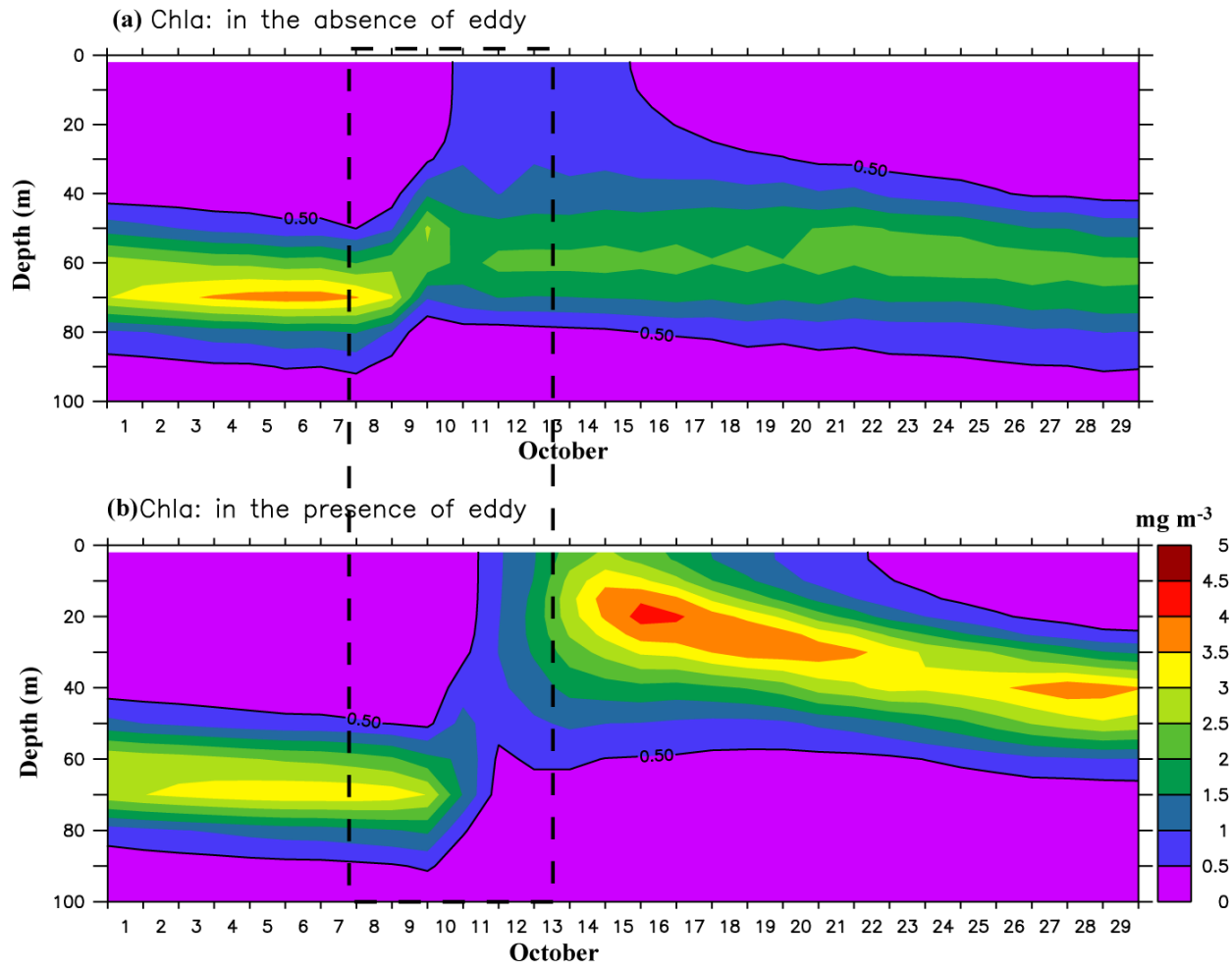


Figure S12. Vertical structure of Chla (a) when eddy was absent (b) when both eddy and cyclone co-exist. Chla in the absence of eddy shown in Figure S12a is averaged over the region shown as a thick black box in Figure 1.